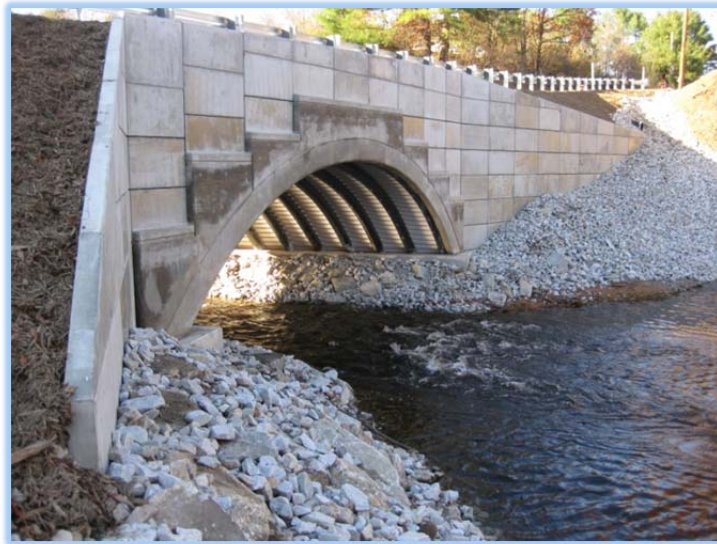




Transportation Research Division



Technical Report 15-04

Bridge-in-a-Backpack™

*Task 8: Investigation of Bridge Performance under
Extreme Temperatures*

Final Report – December 2014

Technical Report Documentation Page

1. Report No. ME 15-04	2.	3. Recipient's Accession No.	
4. Title and Subtitle Bridge-in-a-Backpack™ Tasks 8: Investigation of Bridge Performance under Extreme Temperatures		5. Report Date December 2014	
		6.	
7. Author(s) Keenan Goslin P.E. Ben Pomeroy, Undergraduate Research assistant Habib Dagher, Ph.D., P.E. Keith Berube Ph.D. William Davids Ph.D., P.E.		8. Performing Organization Report No. AEWC Report Number 15-21-1023H	
9. Performing Organization Name and Address University of Maine – Advanced Structures and Composites Center		10. Project/Task/Work Unit No. Project 17891.00 – Task 8	
		11. Contract © or Grant (G) No. Contract # 20111223*2878	
12. Sponsoring Organization Name and Address Maine Department of Transportation		13. Type of Report and Period Covered	
		14. Sponsoring Agency Code	
15. Supplementary Notes			
16. Abstract (Limit 200 words) This report includes fulfillment of Task 8 of a multi-task contract to further enhance concrete filled FRP tubes, or the Bridge in a Backpack. One recurring question has been its performance in fire conditions, mainly small campfires and handheld torches. Previous testing for this technology at the Composites Center has looked at its ignitability using small coupons or sections of the concrete filled arch. This task provides a more extensive look at the performance of this particular composite system. This project consisted of three phases including: laboratory coupon tests; large scale field fire tests of a traditional steel girder and concrete deck specimen and a hybrid composite arch test specimen; and a laboratory structural test to evaluate residual capacity of the composite arches after the field fire test. The principal objective of this project was to compare the performance of the two full scale test specimens when exposed to the same fire environment.			
17. Document Analysis/Descriptors Arch bridges, concrete filled FRP tubes, fire testing, Bridge-in-a-Backpack		18. Availability Statement	
19. Security Class (this report)	20. Security Class (this page)	21. No. of Pages 52	22. Price

Bridge-in-a-Backpack™

Task 8: Investigation of Bridge Performance under Extreme Temperatures

Prepared for:

Dale Peabody P.E.
Director Transportation Research
Maine Dept. of Transportation
16 State House Station
Augusta, ME 04333-0016

University of Maine's Advanced Structures and Composites Center
Report Number: 15 – 21-1023H

December 10, 2014

Prepared by:

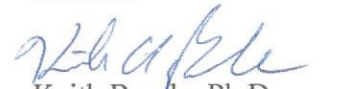


Keenan Goslin P.E.
Structural Engineer

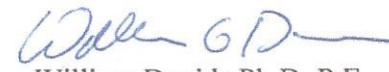
Ben Pomeroy
Undergraduate Research Assistant

Reviewed by:

Habib Dagher Ph.D. P.E.
Director



Keith Berube Ph.D.
Assistant Professor of
Mechanical Engineering
Technology



William Davids Ph.D. P.E.
John C. Bridge Professor of
Civil Engineering

This report shall not be reproduced, except in full, without the written approval of
University of Maine's Advanced Structures and Composites Center.



An ISO 17025 accredited testing laboratory, accredited by the International Accreditation Service.

Table of Contents

EXECUTIVE SUMMARY..... 5

COUPON TESTING 7

Introduction..... 7

Test Plan..... 7

Instrumentation & Equipment..... 9

Flame exposure 9

Results 9

Observations & Discussion 12

Conclusions..... 13

LARGE SCALE TESTING WITH BURN CHAMBER..... 14

Introduction..... 14

Applicable Literature 14

Specimen Design and test preparation 15

Test Setup & Procedure 16

Results 22

Discussion and Specimen Conditions Post Test 34

Conclusions..... 41

LABORATORY STRUCTURAL TESTING OF LARGE SCALE TESTING..... 42

Objective..... 42

Test setup and instrumentation 42

Results 45

Discussion and Conclusions 49

REFERENCES 50

APPENDIX A – CASE STUDY: DESIGN CALCULATIONS FOR EXTREME EVENT II LOADING WITH REDUCED MATERIALS PROPERTIES 51

Figure 1 - Typical Coupon Geometry 7

Figure 2 – Chart of Coupon Strength with Various Flame Exposures 11

Figure 3 - Failure in carbon layer for longitudinal specimens 12

Figure 4 - Failure in glass layer for transverse cut coupons 12

Figure 5 - Failure in carbon layer for longitudinal specimens 12

Figure 6 - Failure in glass layer for transverse cut coupons 12

Figure 7 – Typical exposed sample after exposure for 30 seconds 13

Figure 8 – Bottom mat of reinforcing steel, studs and girders 15

Figure 9 – Decking formed for concrete deck placement 16

Figure 10 – Burn chamber without burner or insulation **Error! Bookmark not defined.**

Figure 11 – Embedded thermocouple locations 17

Figure 12 – Bridge transverse section view at midspan showing embedded
thermocouples’ depth 18

Figure 13 – Thermocouple location on front of burn chamber 18

Figure 14 – Thermocouple location on right and left sides of chamber 19

Figure 15 – String potentiometer locations for steel & concrete bridge 20

Figure 16 – String potentiometer locations for arch test 21

Figure 17 – Oil Burner setup 21

Figure 18 - Interior of chamber prior to steel bridge test 22

Figure 19 – Deflection of steel and concrete bridge 23

Figure 20 – View through peep sight at bottom of steel girder immediately after
turning off burner 23

Figure 21 – Air temperature during testing of steel and concrete bridge 24

Figure 22 – Deck temperatures through the depth of concrete deck in location 1 25

Figure 23– Deck temperatures through the depth of concrete deck in location 2 26

Figure 24– Deck temperatures through the depth of concrete deck in location 3 26

Figure 25– Deck temperatures through the depth of concrete deck in location 4 27

Figure 26– Deck temperatures through the depth of concrete deck in location 5 27

Figure 27 – Individual embedded thermocouples (3” from bottom face of deck) 28

Figure 28 – View through peep sight into chamber during composite arch burn test 29

Figure 29 – Air temperature during heating of hybrid FRP composite bridge 30

Figure 30 – Temperature versus time for gages 21-23 in concrete deck of FRP arch bridge 31

Figure 31 - Temperature versus time for gages 24-26 in concrete deck of FRP arch bridge 31

Figure 32 - Temperature versus time for gages 27-29 in concrete deck of FRP arch bridge 32

Figure 33 - Temperature versus time for gages 30-32 in concrete deck of FRP arch bridge 32

Figure 34 - Temperature versus time for gages 33-35 in concrete deck of FRP arch bridge 33

Figure 35 - Temperature versus time for gages 36-39 in concrete deck of FRP arch bridge 33

Figure 36 – Deflection of midspan string pot during test 34

Figure 37 – Longitudinal deflections in steel girders following the test 35

Figure 38 – View under bridge from within the chamber shortly after the test..... 36

Figure 39 – Arch bridge test smoke production..... 36

Figure 40 – Interior of bridge post test 37

Figure 41 – Arches at interface with chamber 37

Figure 42 – Underside of decking after removal from the arches 38

Figure 43 – Underside of second decking panel after removal from arches 38

Figure 44 – Inner glass layered charred under the dry carbon fiber 39

Figure 45 – Horizontal movement of footings during test..... 40

Figure 46 – Self-reacting system with overhang opposite burner 40

Figure 47 – Bridge test specimen returning to structural testing lab 42

Figure 48 – Arches prior to testing under test frame 43

Figure 49 – String potentiometer locations..... 44

Figure 50 – String potentiometers at shoulders 44

Figure 51 – Typical arch failure at shoulder during structural testing..... 45

Figure 52 – Load versus deflection plots of each arch during structural testing 46

Figure 53 – Footing deflections 47

Figure 54 – Load versus shoulder vertical deflection..... 48

Figure 55 – Applied load versus arch shoulder horizontal deflection 48

Figure 56 – RISA 3D model analysis estimating moment during test 49

Table 1 - Coupon Name Designations 8

Table 2 - Coupon Exposure Condition Nomenclature..... 8

Table 3 – Summary of Tension Test Results for Longitudinal Single Carbon
 Layer Specimens 10

Table 4 – Summary of Tension Test Results for Transverse Single Carbon
 Layer Specimens 10

Table 5 – Summary of Tension Test Results for Longitudinal Double Carbon
 Layer Specimens 10

Table 6 – Summary of Tension Test Results for Transverse Double Carbon
 Layer Specimens 11

EXECUTIVE SUMMARY

The University of Maine's Advanced Structures and Composites Center (the Center) has developed and licensed a hybrid composite arch technology for use in buried arch bridge systems. One recurring question has been its performance in fire conditions, mainly small campfires and handheld torches. Previous testing for this technology at the Composites Center has looked at its ignitability using small coupons or sections of the concrete filled arch. This project provides a more extensive look at the performance of this particular composite system. This project consisted of three phases including: laboratory coupon tests; large scale field fire tests of a traditional steel girder and concrete deck specimen and a hybrid composite arch test specimen; and a laboratory structural test to evaluate residual capacity of the composite arches after the field fire test. The principal objective of this project was to compare the performance of the two full scale test specimens when exposed to the same fire environment.

As there is no current standard for fire performance of bridges, a comparative test was performed where traditional materials were designed for and tested against the same loads and exposure conditions. Two twenty foot long test specimens designed for HL-93 loadings were tested as simple spans by applying a load of 23,125 lbs and exposing the center 6 feet of the span to average temperatures of approximately 1,500 degrees Fahrenheit. The steel and concrete test specimen deflected up to 3.06 inches due to the rising temperature of the steel girders and deck. The test was stopped at 33 minutes when damage to the test chamber would have occurred due to the deflections. The composite arch bridge was tested with similar temperature gradients and the same loading. Deflections were measured at the crown of the deck where a maximum of approximately 1 inch was recorded during the test, which was partially due to outward movement of the footings. The composite arch test was stopped at the planned one hour mark.

Coupon tensile testing was also performed on control and fire exposed samples. These coupons were subjected to varying flame exposures, and then were tensile tested to determine the loss of strength due to fire exposure. The tensile test was performed according to a modified ASTM D3039 with notched 2 inch by 5 inch nominal sized coupons. The fire exposures nominally followed the horizontal Bunsen burner test from the FAA's Aircraft Materials Fire Test Handbook. Longer exposures (300 seconds) beyond the scope of the standard FAA test were also performed to achieve charring that could be expected with larger fires under a bridge. It was found that longitudinal coupons subjected to flame for 300 seconds, which appeared to be long enough for full burn off of the resin, retained roughly half (49.8%) of the peak measured strength of the control coupons. Transverse coupons exposed for 300 seconds retained 63% of the peak measured strength. All hybrid coupons were tested with the carbon layer(s) towards the flame as would be the case in hybrid arches of carbon and glass layers presently in service.

Structural testing of three individual arches from the field fire testing was performed with a point load at the crown and arch bases embedded in self-reacting concrete footings in the Structural Testing Laboratory at the Composites Center. An average load of 9.84 kips was required to

cause failure which occurred at the interface of damaged and undamaged laminate. This was the location where the insulation in the wall of the fire chamber was placed. A simple beam-element finite-element model of the fire damaged arch subjected to this loading predicts a moment at failure of approximately 45.5 kip-in. A previously developed and experimentally verified sectional model of the arch cross-section predicts a bending capacity is 187 kip-in for an undamaged arch.

A case study was also conducted to evaluate a hypothetical 40 foot span arch bridge with a 15 foot rise and 5 foot arch spacing. Analyses were performed for Strength I and Extreme II load cases comparing internal moments. Bending capacities were calculated for a cross section with 2 carbon longitudinal layers similar to several in-service bridges and compared to the Strength I case. The same analysis was conducted with a 50% reduction in tensile strain to failure, according to the minimum retained coupon strength test results, and that capacity was compared to the internal moments from the Extreme II load case. Peak Strength I internal moments for this configuration were 495.3 kip-in where the factored nominal moment capacity was 530.4 kip-in. Extreme II internal moments for this configuration were 322.3 kip-in with a factored nominal moment capacity with 50% tensile capacity of 399.7 kip-in. Cross section failure modes changed from the full capacity (compression) to the half capacity section (tensile rupture).

A hybrid composite arch system for buried arch bridges has been developed by the University of Maine's Advanced Structures and Composites Center (the Composites Center) and is commercialized by Advanced Infrastructure Technologies, LLC (AIT) who designs, manufactures and sells the composite bridge systems. The bridge uses a hybrid composite arch comprised of a laminated composite tubular arch filled with concrete. The laminate has been constructed with several layers of carbon and glass fibers or just glass fabrics and infused with a vinyl ester resin.

Historically concerns have been raised regarding the combustibility and performance of composites when exposed to fire conditions. AIT and the Composites Center have fielded questions regarding this topic. Previous testing at the Composites Center was conducted on disks of concrete-filled FRP tubes with a Bunsen burner and showed it was much harder to ignite the concrete filled disk than it was the laminate (Demokowicz 2012). This project was conducted to investigate more extensively some of the questions regarding fire performance of these particular composite bridges. The testing project consists of three tasks. They include: laboratory coupon testing of fire exposed coupons in tension; full scale comparative field testing of two half-width bridges using composites and steel; and residual strength testing of the full scale composite arches in the structural testing laboratory.

COUPON TESTING

INTRODUCTION

The hybrid composite arch bridge system uses concrete arches that are formed with a laminate of either a hybrid carbon and glass fiber reinforced polymer (FRP) or glass FRP. The fabrics in the laminates are braided with the inner glass layer setting the diameter and confining the concrete in the arches and the outer layers providing flexural reinforcement and protection for the concrete. This report summarizes tensile tests of fire exposed laminate coupons from witness plates representative of bridges in service today using the buried hybrid composite arch technology. The loss of strength due to extreme heat was investigated and is presented here.

TEST PLAN

Testing of the coupons nominally followed two different test standards: ASTM D3039 for tensile strength, and the Horizontal Bunsen Burner test described in the FAA's Aircraft Materials Fire Test Handbook. The FAA standard is intended to evaluate the ability of materials to ignite and for flames to propagate, but was expanded for use here to expose coupons to a practical flame condition under bridges.

Coupons were cut from a plate of laminated composite. All coupons were 2 inches wide and 5 inches long nominally, with transverse notches cut mid-length as shown in Figure 1. The width of the coupon at the mid-point is nominally 1 inch. This is a modified coupon from the ASTM D3039 tension standard and ensures that tows of carbon fiber in the failure section of the coupon are clamped in the grips of the test machine.



Figure 1 - Typical Coupon Geometry

The carbon tows are nominally oriented $\pm 22^\circ$ off of the longitudinal axis, and the glass tows are oriented $\pm 81^\circ$ off of the longitudinal axis of the composite plate in these coupons. Samples were cut from the composite plate in both the longitudinal and transverse directions, and tested in tension in these directions to assess the longitudinal and transverse tensile strengths.

In this investigation, four different types of coupons were tested. These four types reflected variation on two parameters as shown in Table 1. These two parameters were:

- 1) Longitudinal vs. Transverse orientation
- 2) Single vs. Double ply carbon layer. For all coupons, there was only a single glass layer.

Table 1 - Coupon Name Designations

	Longitudinal	Transverse
Single ply CFRP	1L (Long)	1T (Trans)
Double ply CFRP	2L (Long 2)	2T (Trans 2)

Coupons were exposed in the Bunsen burner with two variables. These two variables were:

- 1) Duration of exposure: 30 s, 60 s, and 300 s exposure times
- 2) High vs. Low position with regard to the test flame. The High position was 1.5 inches above the tip of the Bunsen burner. The Low position was 0.75 inches above the tip of the Bunsen burner.

The nomenclature for exposure conditions is given in Table 2.

Table 2 - Coupon Exposure Condition Nomenclature

	High	Low
30 seconds	30_HI	30_LO
60 seconds	60_HI	60_LO
300 seconds	300_HI	300_LO
Control	C	

Thus, for each of the four types of coupons, there were 7 treatments, with 5 samples each with the exception of the 2L type, for which there was a sufficient amount of samples to only complete 3 repetitions for each treatment. Each sample was then tested in tension to evaluate strength variations with fire exposures.

The combined nomenclature for specimen identification can be seen printed on each sample as in Figure 1. For example, a sample that reads *FT_1L_30_LO* indicates the following: *FT* denotes fire test; *1L* indicates 1 layer of carbon fiber with the coupon cut in the longitudinal orientation;

30 denotes a 30 second exposure time, and *LO* indicates the lower sample placement in the flame.

INSTRUMENTATION & EQUIPMENT

A sealed flame chamber (AS HVUL) was used at the Composites Center to expose the fire test specimens. A common stop watch was used to measure the duration of the test.

A 22 kip Instron servo-hydraulic actuator and calibrated 22 kip load cell (AS 1085) were used to load the specimens and measure both deflection and load respectively. Data was collected at 5 hertz. The specimens were loaded with a constant speed of 0.05 in/min.

FLAME EXPOSURE

The specimens were exposed to a flame from a methane-fueled Bunsen burner with the flame adjusted to a height of 1-1/2 inches, as specified by the FAA Aircraft Materials Fire Test Handbook. A specimen support was chosen that allowed the flame to contact the center notched portion of the specimen. The support did not shield the center portion of the coupon from the flame.

The specimen support was brought to the desired height, either 0.75 inches above the base of flame for the *LO* treatment, or 1.5 inches above the base of flame for the *HI* treatment. The exhaust fan was turned off for all treatments except the 300_*LO* treatment to ensure a steady consistent flame. The exhaust fan of the burn chamber was turned on during exposure of the 300_*LO* coupons to prevent a buildup of smoke outside the fume hood. This appeared to reduce heating of the coupons, as discussed later. Groups of specimens were exposed to the flame treatment and then stored in 70°F and 50% relative humidity until tensile testing, which was generally conducted within 24 hours of the flame test.

RESULTS

The results from tensile testing are presented in Table 3, Table 4, Table 5 and Table 6. The specimens in each table are grouped by coupon type including 1 layer of carbon in the longitudinal direction (1L), 1 layer of carbon in the transverse direction (1T), 2 layers of carbon in the longitudinal direction (2L), and 2 layers of carbon in the transverse direction (2T), respectively. The average strength, standard deviation of strength and coefficient of variation of strength are given. Strength was calculated as peak load divided by the cross sectional area of the notched section of the coupon. The percent retention is also given for each coupon set. Strength values should be used for comparisons only in each group in this report. The minimum strength retention across all four coupons' groups was 49.8%, which corresponded with the single layer of carbon hybrid laminate exposed for 300 seconds in the lower (hotter) position. The data also is shown graphically in Figure 2. The error bars in the bar graph represent one standard deviation to each side of the mean.

Table 3 – Summary of Tension Test Results for Longitudinal Single Carbon Layer Specimens

Type: 1 Layer Longitudinal	Average Strength (ksi)	Standard Deviation (ksi)	COV (%)	Number of Samples	% Retention
30_LO	123.4	7.78	6.3	5	102.0%
30_HI	115.3	11.40	9.9	5	95.4%
60_LO	117.9	8.59	7.3	5	97.6%
60_HI	118.1	7.31	6.2	5	97.8%
300_LO	60.1	2.59	4.3	5	49.8%
300_HI	68.1	2.30	3.4	5	56.4%
C	120.8	10.60	8.8	5	100%

Table 4 – Summary of Tension Test Results for Transverse Single Carbon Layer Specimens

Type: 1 layer Transverse	Average Strength (ksi)	Standard Deviation (ksi)	COV (%)	Number of Samples	% Retention
30_LO	50.1	3.16	6.3	5	96.4%
30_HI	51.6	2.48	4.8	5	99.2%
60_LO	48.7	3.07	6.3	5	93.7%
60_HI	46.2	2.88	6.2	5	88.9%
300_LO	32.8	4.67	14.2	12	63.1%
300_HI	29.8	1.50	5.0	5	57.3%
C	52.0	2.72	5.2	5	100%

Table 5 – Summary of Tension Test Results for Longitudinal Double Carbon Layer Specimens

Type: 2 layer Longitudinal	Average Strength (ksi)	Standard Deviation (ksi)	COV (%)	Number of Samples	% Retention
30_LO	144.6	24.2	16.7	3	86.1%
30_HI	152.6	14.5	9.5	3	90.9%
60_LO	154.5	15.1	9.8	3	92.0%
60_HI	144.9	5.8	4.0	3	86.3%
300_LO	85.3	12.7	14.8	7	50.8%
300_HI	131.5	7.4	5.6	3	78.3%
C	167.9	5.1	3.0	3	100%

Table 6 – Summary of Tension Test Results for Transverse Double Carbon Layer Specimens

Type: 2 Layer Transverse	Average Strength (ksi)	Standard Deviation (ksi)	COV (%)	Number of Samples	% Retention
30_LO	38.7	1.88	4.9	5	99.2%
30_HI	38.9	2.05	5.3	5	99.6%
60_LO	37.9	1.08	2.8	5	97.2%
60_HI	38.6	1.12	2.9	5	98.9%
300_LO	24.0	2.70	10.8	7	64.1%
300_HI	26.6	7.22	27.1	5	68.3%
C	39.0	1.64	4.2	5	100%

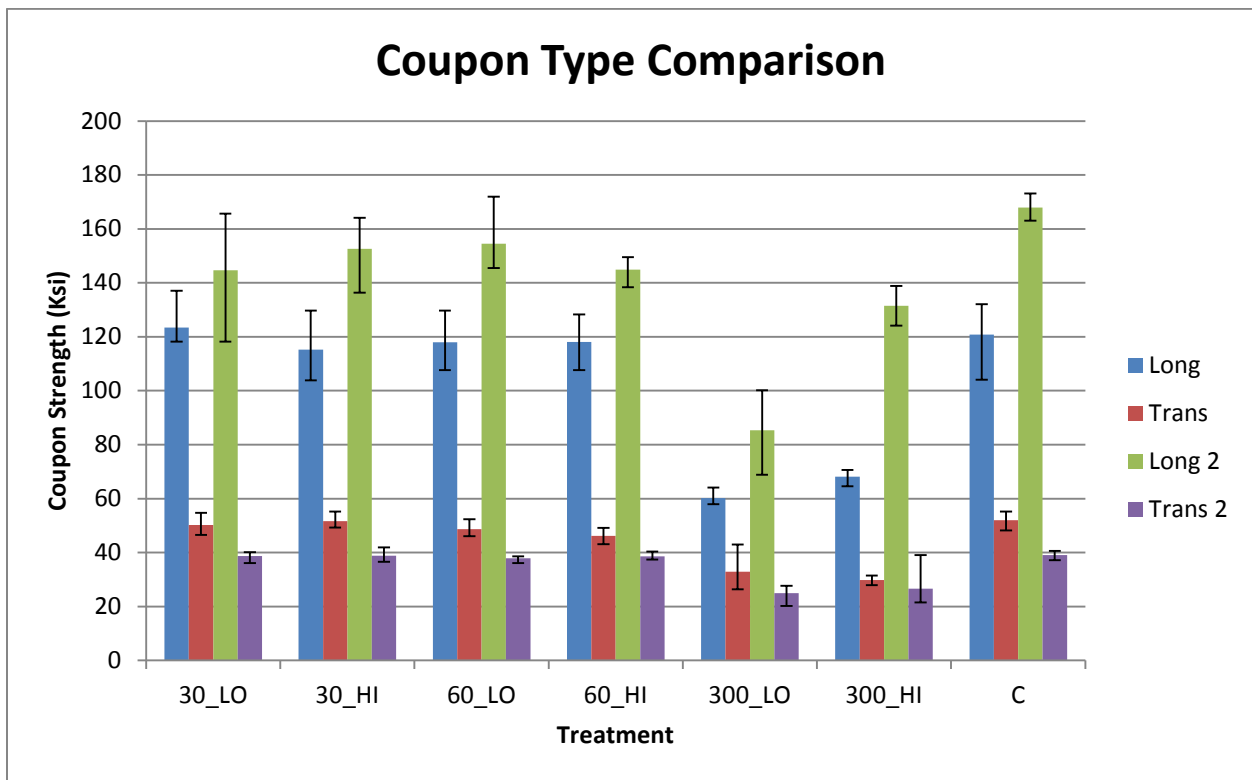


Figure 2 – Chart of Coupon Strength with Various Flame Exposures

All coupons failed first in the rupture of the fibers nominally in the longitudinal axis of the coupons, which was the desired mode of failure. This is shown in Figure 3 and Figure 4 and again in Figure 5 and Figure 6.



Figure 3 - Failure in carbon layer for longitudinal specimens



Figure 4 - Failure in glass layer for transverse cut coupons

OBSERVATIONS & DISCUSSION

Ignition of the coupons occurred at approximately 60 seconds for coupons in the high position, and at approximately 50 seconds for coupons in the low position. After ignition, the coupons burned for 2 to 3 minutes then self-extinguished, leaving an approximately 2 inch diameter circle of charred material around the center of the coupon, as seen in Figure 7. Coupons exposed for 300 seconds showed significantly more charring and dry fabric could be seen on the surface.



Figure 5 - Failure in carbon layer for longitudinal specimens



Figure 6 - Failure in glass layer for transverse cut coupons



Figure 7 – Typical exposed sample after exposure for 30 seconds

Variations in coupon strengths seen could partially be attributed to variations in flame temperature due to variations in flame height and air circulation in the lab and fume hood. Ignition of the 300_LO samples was delayed by up to 10 seconds due to the removal of heat caused by having the exhaust fan on in the fume hood.

CONCLUSIONS

The data shows little to no statistically significant change in coupon tensile strength in response to 30 and 60 second flame exposures. There is a drastic change in tensile strength for those coupons subjected to 300 second exposures. This is consistent with the observations during testing.

After the 300 seconds of exposure, the laminate retains approximately 50% of its original tensile strength. Transverse coupons retained higher tensile strengths when compared to their controls. It should be noted however, that the glass layer was always on the back of the coupon during flame exposure and therefore may not have been exposed to the same extent as the front face did in direct flame.

LARGE SCALE TESTING WITH BURN CHAMBER

INTRODUCTION

Coupon testing has been conducted which quantified the laminate degradation under laboratory fire conditions. A full scale fire test of a bridge system was designed to evaluate its performance under fire or high heat conditions. As there were no applicable specifications on bridge performance during fire conditions, a comparative test was conducted with the traditional bridge construction materials of steel and concrete. Applicable literature was reviewed in designing the test as well as designing both test specimens. Each specimen was designed to the same structural loads so there can be a fair comparison of results.

APPLICABLE LITERATURE

The design of the comparative full scale fire test started with a literature search for applicable test standards, similar test programs, and design standards for fire performance of bridges. Fire performance of bridges has been a topic of discussion and research for several years, but no performance specification existed at the time of this study prescribing the design of bridges for fire. Test standards also do not exist for the fire testing of components of bridges.

According to Kodur et al (2010), “there are no methodologies or design tools for realistic evaluation of bridge response under fire conditions”. Kodur et al (2010) highlight the needs for specific research and development including: the adoption of specific fire scenarios to be used for analysis; the establishment of performance based fire safety design strategies and relevant protection measures; the development of enhanced assessment and repair techniques for damaged bridges; establishment of high temperature properties for new construction materials; and the introduction of new passive methods to enhance performance. They also highlight that there have been several incidents in recent years that have included bridge collapse due to fire across the country, and that critical bridges can be designed to have satisfactory fire resistance that could save time and money in the event of an incident. The study notes that 3 times as many bridges have collapsed due to fire than seismic events and yet the research funding is drastically different for these two programs. Ultimately, there is a threat to bridges as a whole from fire and there needs to be research programs to address these concerns. This test program addresses some of the recommendations from this paper through laboratory and field testing. References from Kodur et al (2010) include ASTM E1529 where a time and temperature curve for a hydrocarbon fueled fire is given.

ASTM E1529 “Standard Test Methods for Determining Effects of Large Hydrocarbon Pool Fires on Structural Members and Assemblies” and ASTM E119 “Standard Test Methods for Fire Tests of Construction and Building Materials” were used as a basis for the design of the full scale fire test program of the hybrid composite arch bridge system. Instrumentation requirements and time temperature curves from these test standards were used to design the test setup and temperature curve for the test.

SPECIMEN DESIGN AND TEST PREPARATION

Two test specimens were constructed. Each was a 20 foot long, 6 foot wide bridge designed for AASHTO HL-93 loads according AASHTO LRFD Bridge Design Specifications (2012), AASHTO LRFD Guide Specifications for Design of Concrete-Filled FRP Tubes for Flexural and Axial Members (2012).

The steel and concrete test specimen was built with two W12x26 steel girders with a composite 7 inch thick concrete deck, and supported as a simple span. The girders can be seen in Figure 8 during construction with only the bottom mat of reinforcing bars and studs in place at that time.

The composite arch bridge was built with four (4) 6.5” diameter hybrid carbon fiber composite concrete filled tubular arches. Two layers of braided carbon fiber served as the outer layers where they provided tensile reinforcement for the cross section. An approximately six (6) foot square FRP composite and unreinforced concrete deck was placed on top of the arches as seen in Figure 9 (concrete formed but not placed in this photo). The composite decking is a commercially available pultruded glass FRP with a urethane resin.



Figure 8 – Bottom mat of reinforcing steel, studs and girders



Figure 9 – Decking formed for concrete deck placement

TEST SETUP & PROCEDURE

A five-sided box steel burn chamber (Figure 10) was constructed for the test (6'-0" W x 6'-0" L x 4'-0" H). The test setup consisted of the scaled bridge specimen, the burn chamber, and some calibrated concrete blocks used as a static load. The burn chamber was placed below the bridge deck, such that the bridge deck acted as the top of the burn chamber, as seen in Figure 11, Figure 13 and Figure 14. Once the bridge specimen and burn chamber were in place, the static load was then applied to the bridge deck prior to firing up the burn chamber. The burn test was conducted until it hit one of three limits. The three limits were: 1) the time of one hour, 2) until bridge failure occurred or 3) a safety limit was reached.



Figure 10 – Burn chamber without burner or insulation

A total of 20 Omega type-K thermocouples were embedded in the bridge deck. The locations of the thermocouples in the slab of the steel bridge are shown in Figure 11 and Figure 12. Each point contains up to three thermocouples. These thermocouples are located at one, three and five inches up from the bottom surface of the bridge deck. A table of their embedment depths is given in Table 7. The thermocouples were placed in three columns across the bridge deck with one column located at the centerline of the bridge and the other two at 22 inches to the left and right of the centerline. Each row has a spacing of 22 inches.

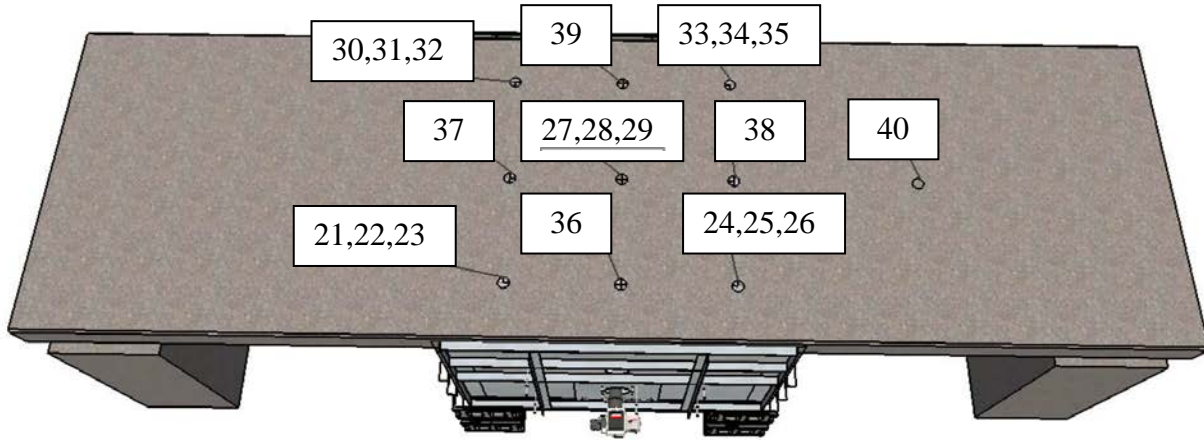


Figure 11 – Embedded thermocouple locations

Table 7 – Depth of Embedded Thermocouples

Sensor No. / Depth to Bottom	5 inches	3 inches	1 inch
N/A	21,24,27,30,33	22,25,28,31,34 36,37,38,39,40	23,26,29,32,35

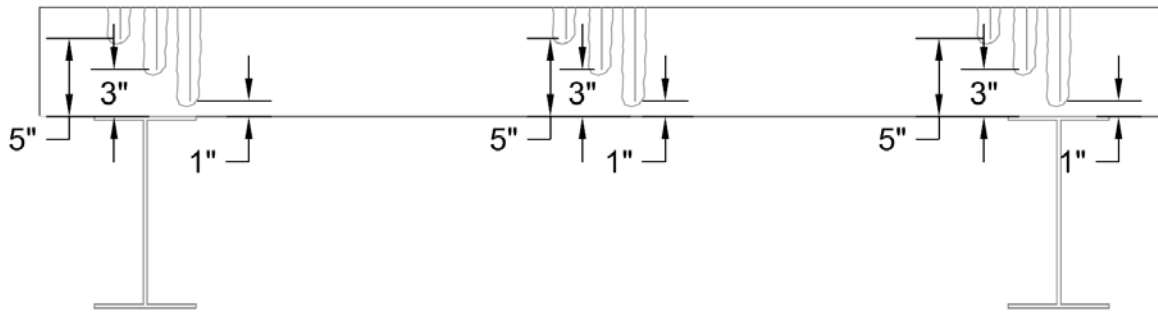


Figure 12 – Bridge transverse section view at midspan showing embedded thermocouples' depth

Fourteen thermocouple probes were placed inside the burn chamber to measure the internal air temperature. Figure 13 and Figure 14 show the placement of the thermocouples. Thermocouple placement is symmetric on either side of the chamber (right and left, front and back) and was the same for the steel bridge and composite bridge decks.

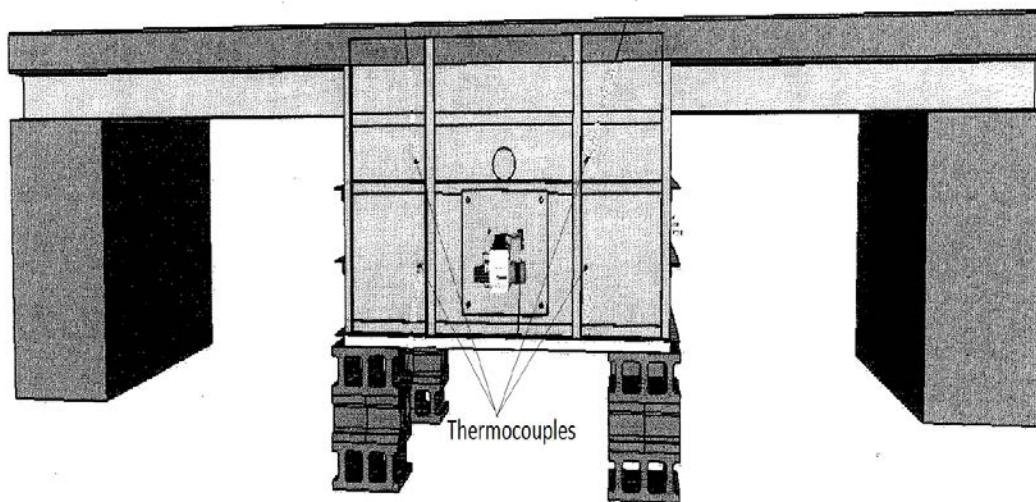


Figure 13 – Thermocouple location on front of burn chamber

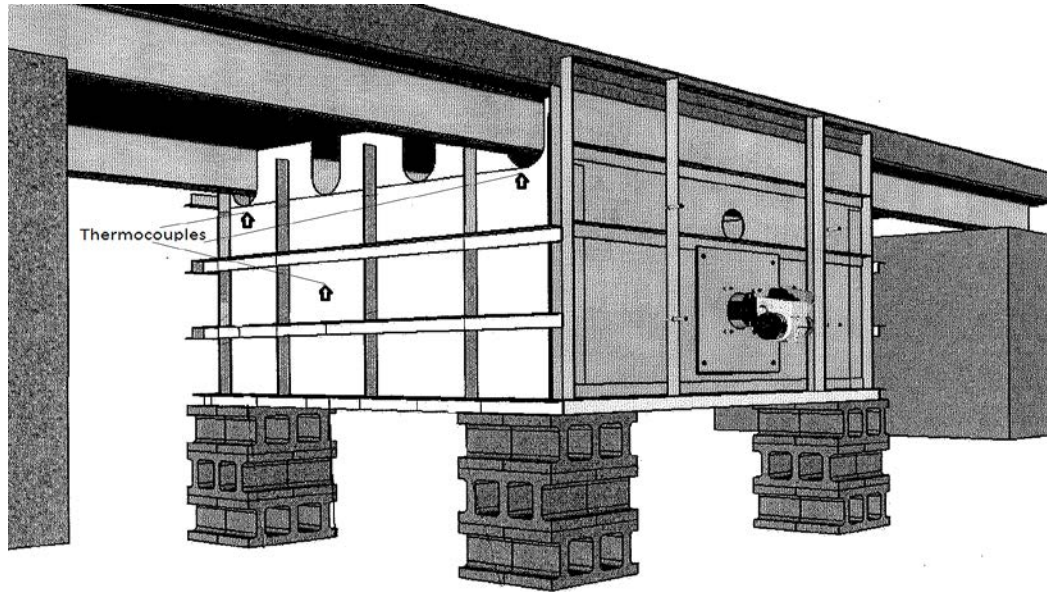


Figure 14 – Thermocouple location on right and left sides of chamber

String potentiometers (pots) were located along the centerline of the bridge span to measure the bridge deflection. For the steel bridge, SP1 (string pot 1) & SP5 were located 18 inches in from the left and right ends of the bridge, respectively when facing the burner side of the bridge. SP2 & SP4 were located 23 inches in from the left and right sides of the bridge, respectively. The final string pot, SP3, was placed at the center line and mounted to the center loading block. The string pot locations can be seen in Figure 15 for the steel and composite bridge specimens, respectively.

The bridge was tested under a constant load of 23,125 lbs as seen in Figure 16. The loading consisted of five precast concrete blocks that were weighed with a calibrated crane scale when placed on the test specimen. This loading was selected to closely represent 19.3% of the affective undamaged live load capacity of the bridge with no factors. The moment due to the blocks nominally equals the nominal moment capacity of the composite bridge section, M_n , minus the moment due to the bridge self-weight. This percentage was chosen as a practical load that could be applied to both the steel and hybrid FRP arch bridges and is 112% of the dead load moment.

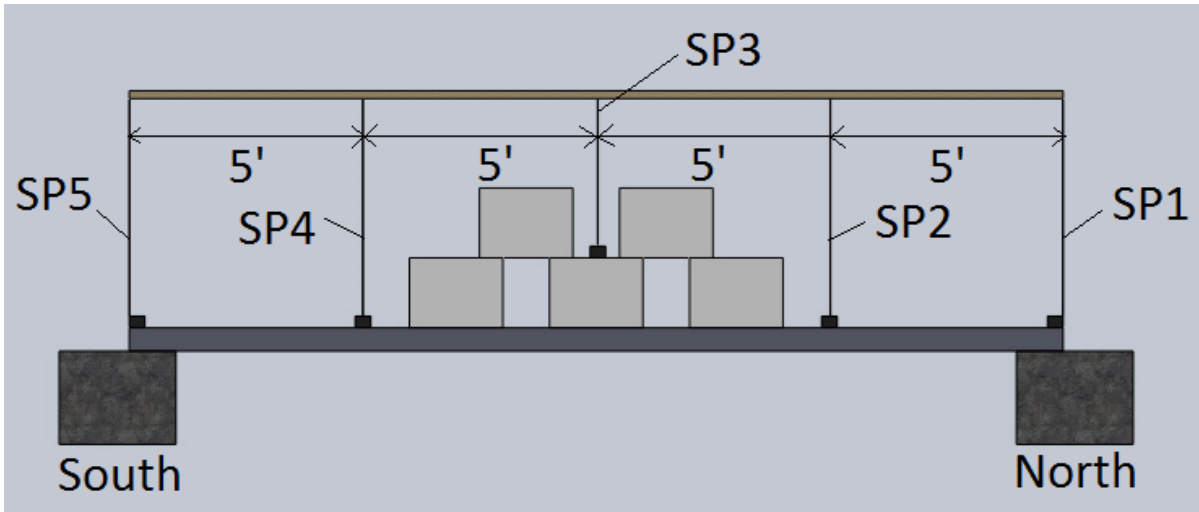


Figure 15 – String potentiometer locations for steel & concrete bridge

String pots were mounted above the composite arch specimen at the same points on the wooden frame support above the specimen as were used for the steel and concrete specimen. SP1 and SP5 though were attached to the arches at the same points as SP2 and SP4 respectively 5 feet from midspan such that two string pots were attached to that single point and vertical and horizontal deflections could be calculated from the measurements. String pots were attached to the first interior arch from the burner side of the chamber (front) as seen in Figure 16.

Temperature and bridge deflection data were recorded throughout the duration of the test. The temperature data was recorded using an IoTech Tempscan 64-channel data acquisition system, while the sting pot data was recorded with a National Instruments SCXI 1600 data acquisition system (AS 541). Data was recorded at a sampling rate of 5 Hz.

The burner for the chamber was a commercial oil burner with a low and high setting. The three options allowed for it to be off (zero BTU's), low (approx. 956,000 BTU's) and high (approx. 1,560,000 BTU's) during the test. The burner was controlled remotely near the instrumentation controls during the test. The burner was mounted on a custom fabricated rolling cart allowing for it to be pulled from the test if structural failure was imminent. A lanyard was attached to the cart as seen in Figure 17.

The five internal sides of the chamber were insulated with Fiberfrax Refractory Ceramic Fiber Insulation. The insulation can be seen in Figure 16, Figure 17 and Figure 18.

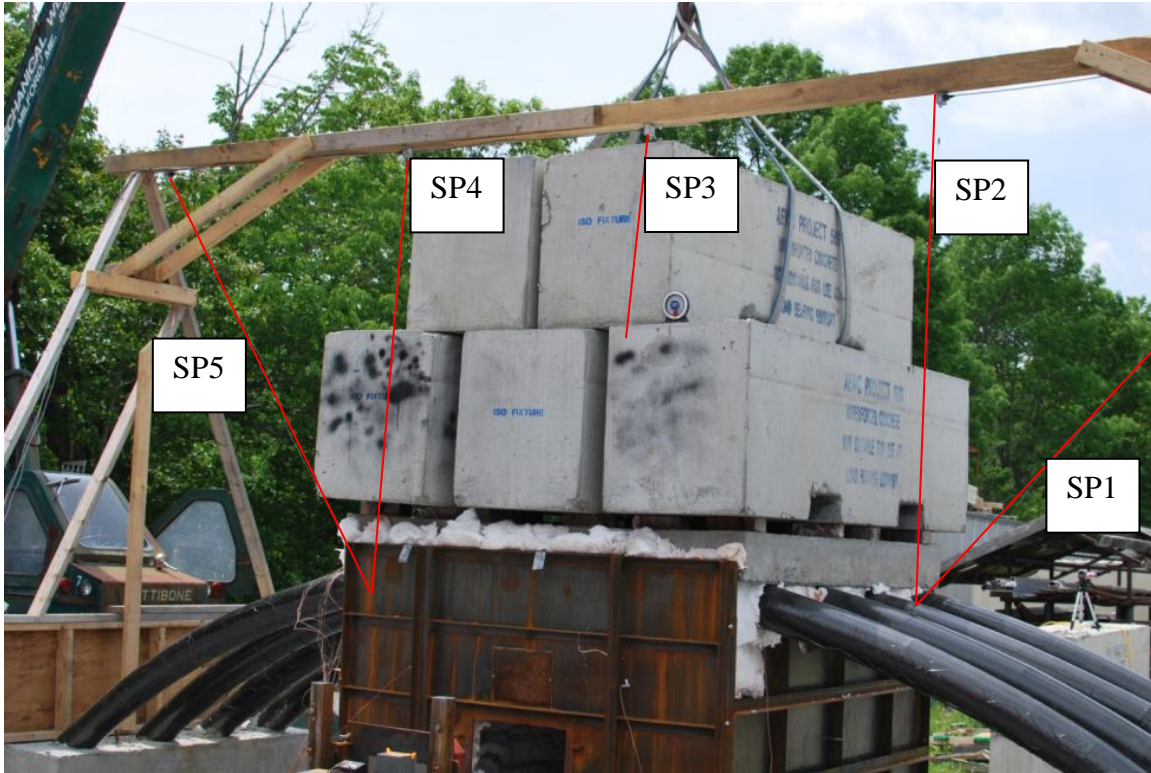


Figure 16 – String potentiometer locations for arch test

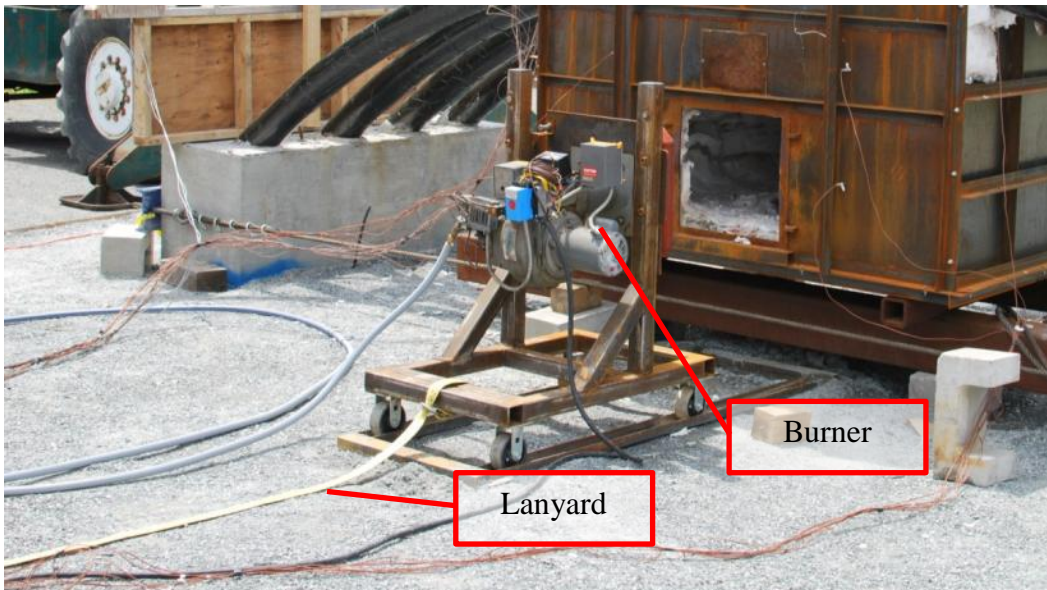


Figure 17 – Oil Burner setup



Figure 18 - Interior of chamber prior to steel bridge test

RESULTS

A burn test was performed on each of the two bridge specimens, with the burner running for 33 minutes during the steel bridge test and 60 minutes during the FRP bridge test. Neither bridge collapsed during the test. The steel bridge test was stopped at 33 minutes as it hit the deflection limits of the burn chamber. The arch bridge test was stopped at the planned 60 minute mark. The steel bridge was tested on June 6th, 2014 and the FRP arch bridge was tested on June 17th, 2014. June 6th was a cool, cloudy day with occasional rain showers. June 17th was a mostly sunny, warm day with clear skies and light winds.

Steel Girder Bridge

Deflections and air temperatures were monitored continuously during the test. Deflections of the steel bridge test can be seen in Figure 19 where the maximum deflection, SP3, was at the midspan. The deflections grew quickly early in the test, but the rate of deflection slowed as the test progressed. A peep sight provided views up into the chamber, which allowed a webcam to capture video throughout the test. Figure 20 shows the glowing steel girder immediately after the burner was turned off indicating the high temperature of the steel girders. The air temperature recorded by each of the probes inside the chamber can be seen in Figure 21 and ranged between approximately 1400°F and 1600°F once the burn chamber got up to temperature. The sawtooth pattern of the air temperature is due to cycling the burner from low to high to maintain the desired air temperature during the test. Some sensors were not plotted due to expected errors in data collection. Temperatures during the test were not uniform throughout the chamber, with areas toward the back (directly in line of the burner nozzle) receiving the most heat, and the front corners being the coolest.

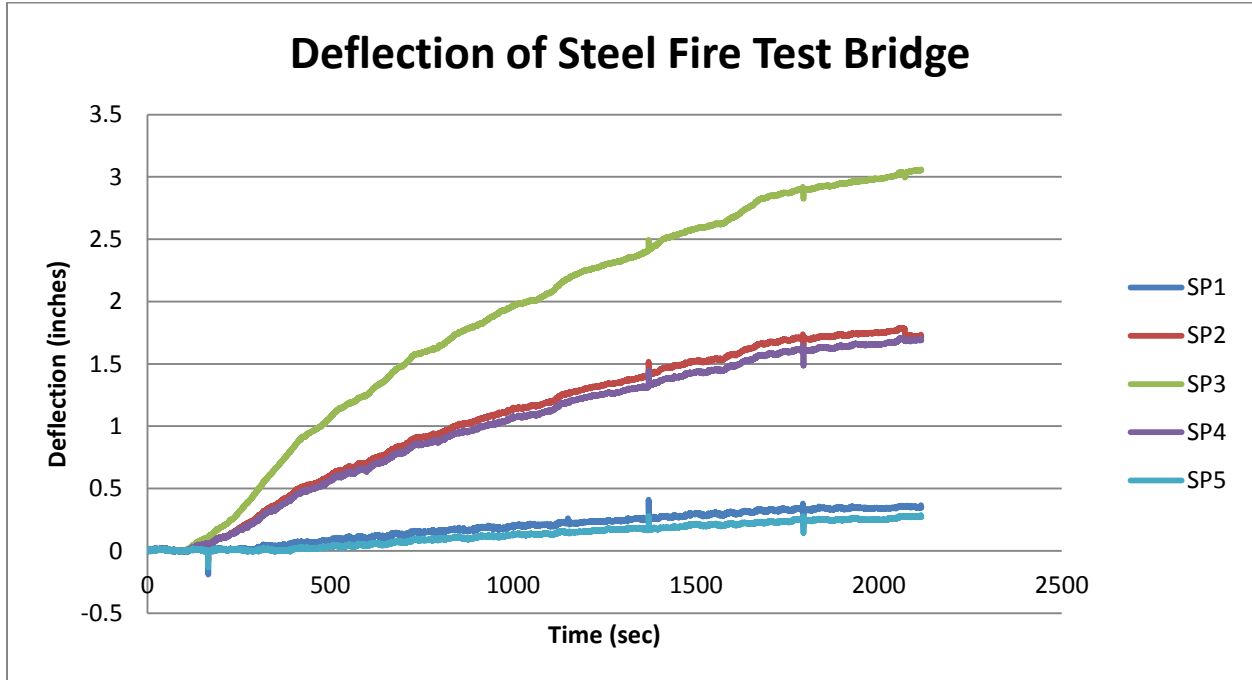


Figure 19 – Deflection of steel and concrete bridge

The location of the thermocouples in the burn chamber are given in Table 8 where the number is given for location on each of the faces of the burn chamber. The front and back at four sensors where the sides had 3 sensors. Two sensors on each side were placed close to the underside of the structural members.

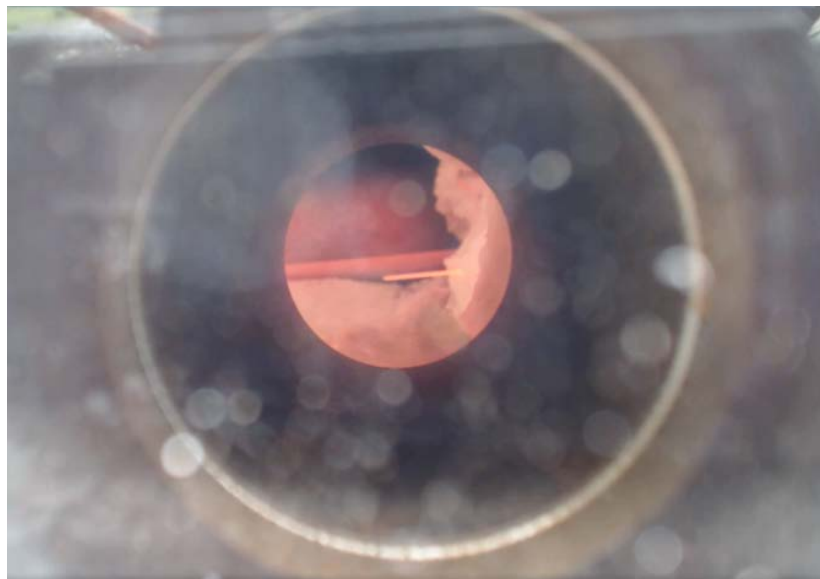


Figure 20 – View through peep sight at bottom of steel girder immediately after turning off burner

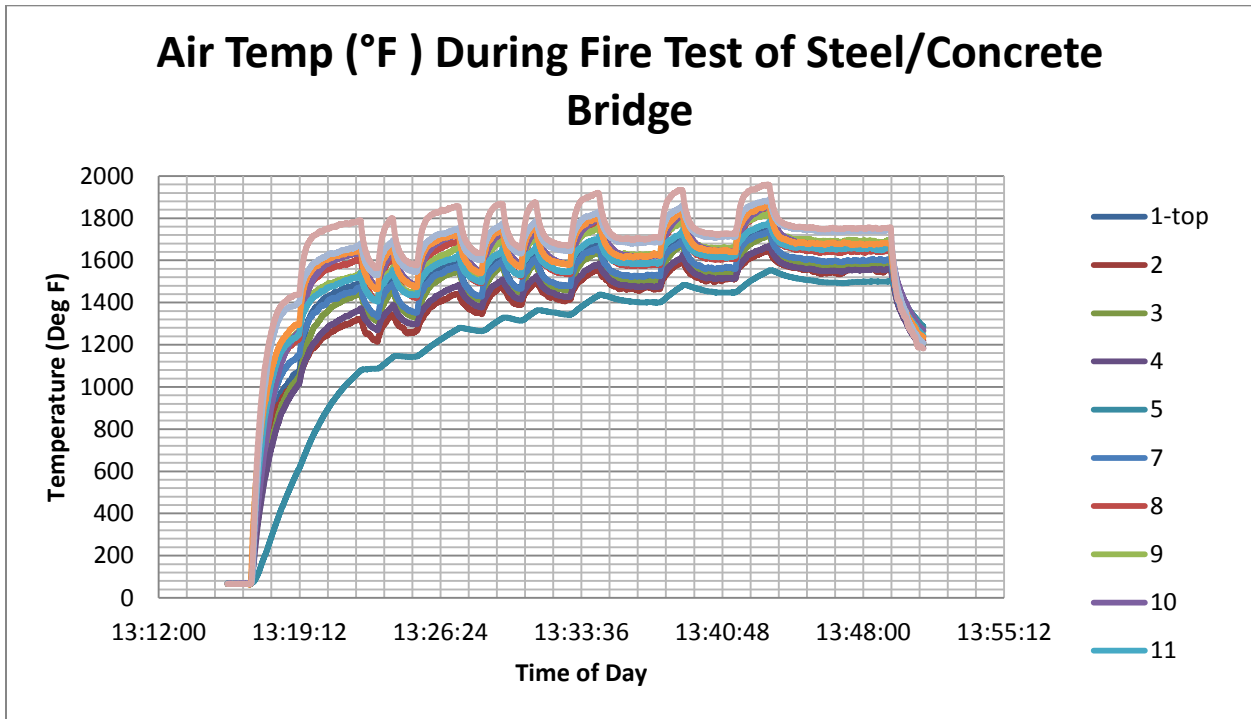


Figure 21 – Air temperature during testing of steel and concrete bridge

Table 8 – Location of Air Temperature Thermocouples

	Top Right	Top Left
	Bottom Right	Bottom Left
Front	2	1
	4	3
Right	9	5
	7*	
Back	12	11
	14	13
Left	10	6
	8*	

*Centered on side wall

Concrete deck temperatures were also recorded at the three depths in the cross section at various points of the deck. The locations of the embedded thermocouples can be seen in plan and section views in Figure 11 and Figure 12, respectively. Each of the plots in Figure 22, Figure 23, Figure 24, Figure 25 and Figure 26 give the temperature measured for that cross section at depths of 1 inch, 3 inches and 5 inches up from the bottom of the deck. There are some unaccounted for spikes in channel 24 but in general temperatures during this test appeared to plateau in the lower depths of the deck between 180°F and 220°F. Temperature variations at points farther from the bottom surface of the deck showed negligible increases in temperature though temperatures did not plateau in all cases. It is expected that the light rain on the test day had an impact on the deck temperatures during the test. Individual sensors placed in the deck are also shown in Figure 27. Sensor 40 is located outside of the burn chamber.

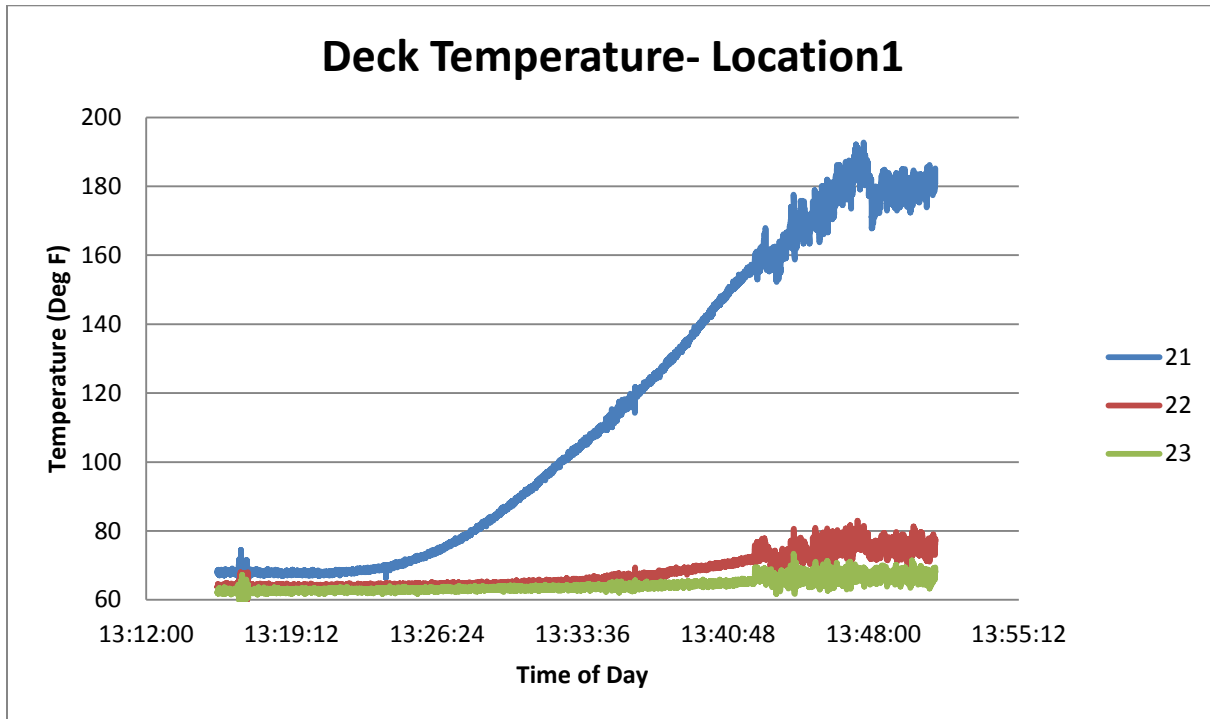


Figure 22 – Deck temperatures through the depth of concrete deck in location 1

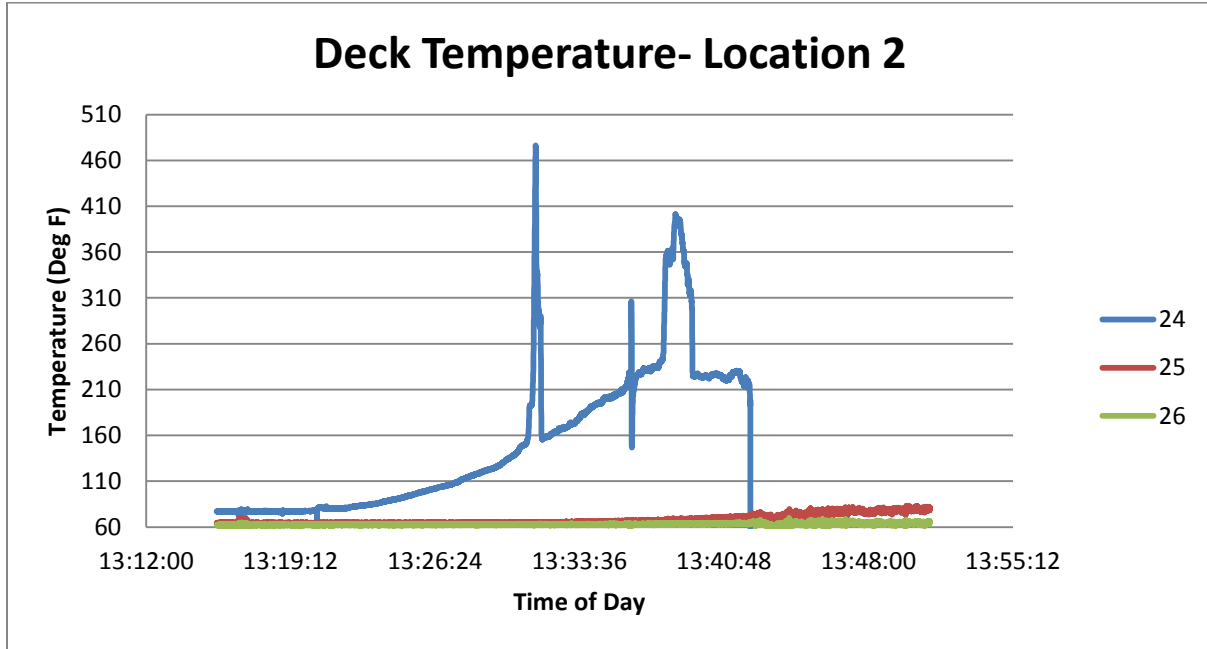


Figure 23– Deck temperatures through the depth of concrete deck in location 2

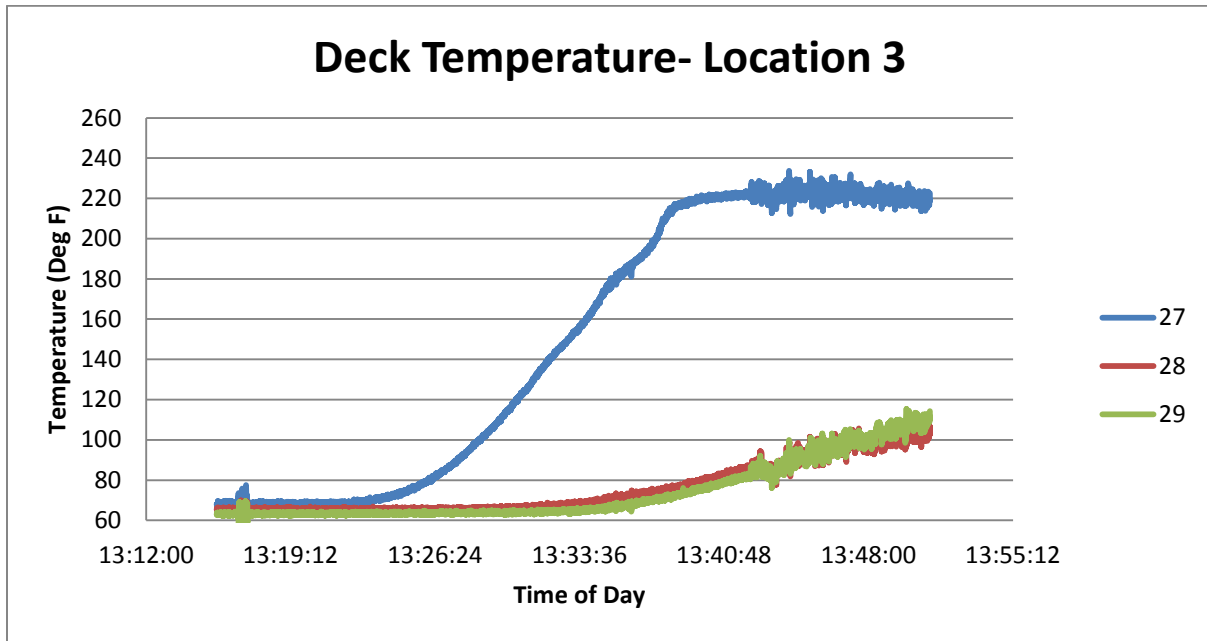


Figure 24– Deck temperatures through the depth of concrete deck in location 3

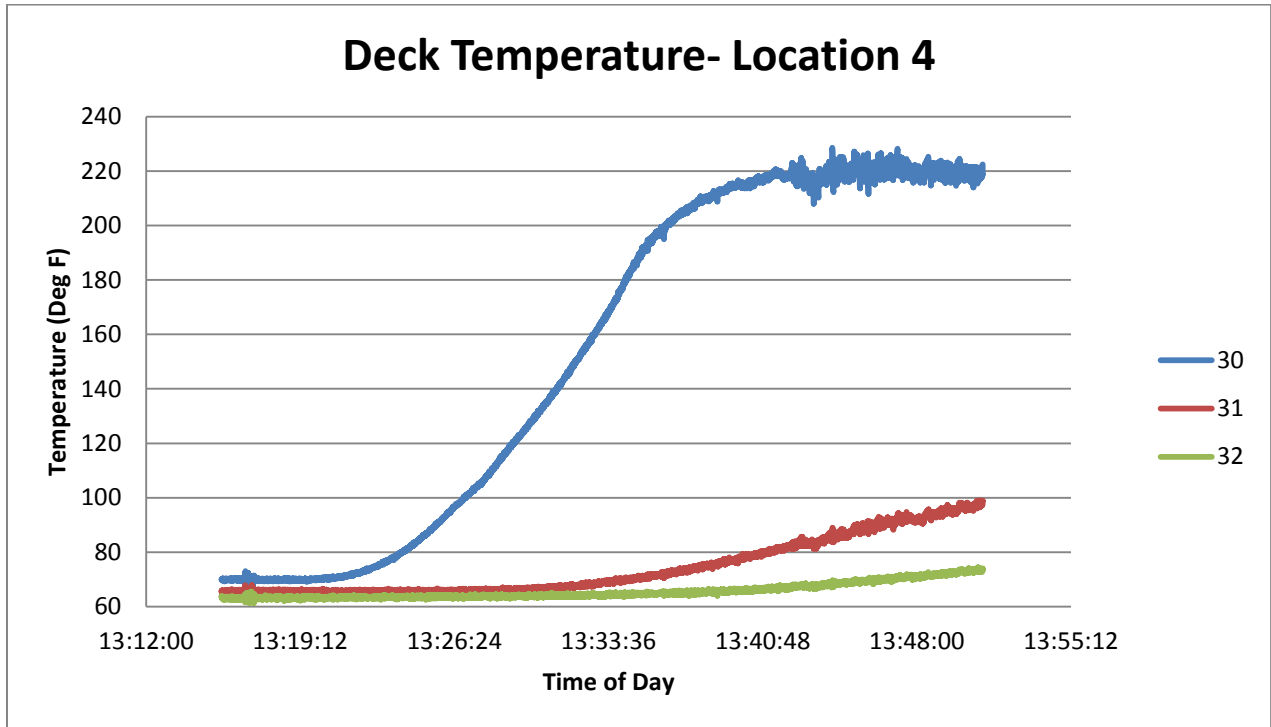


Figure 25– Deck temperatures through the depth of concrete deck in location 4

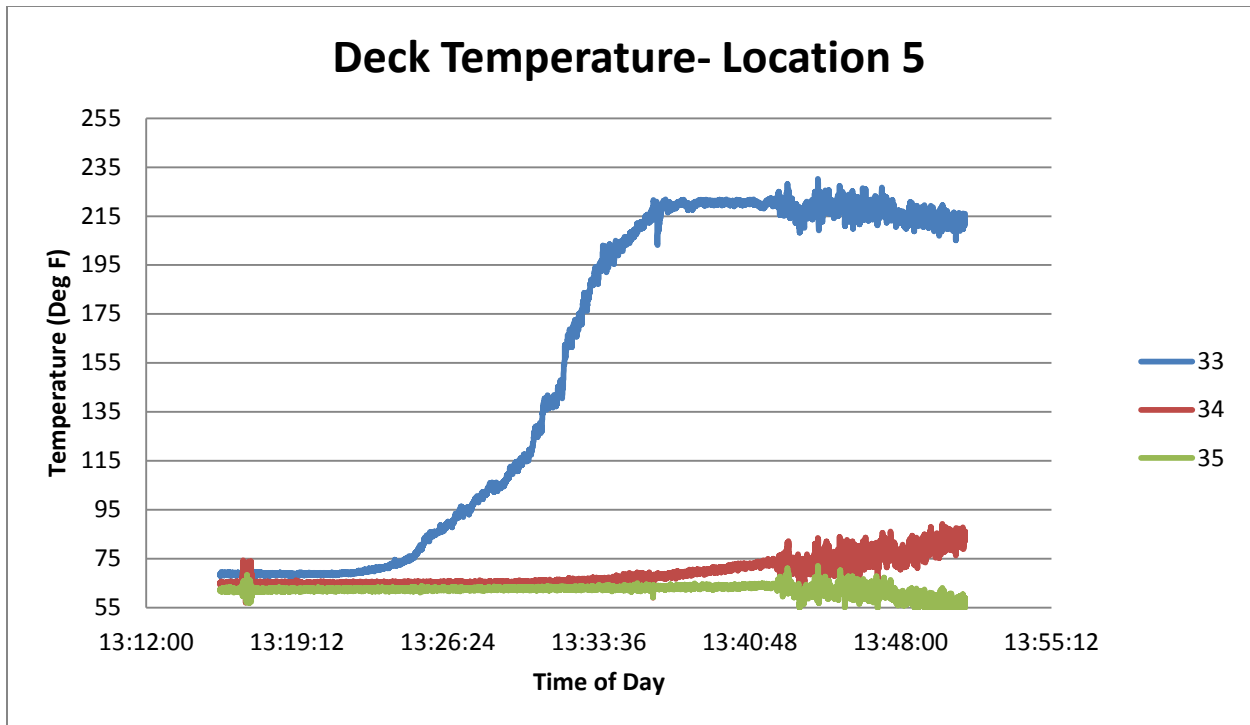


Figure 26– Deck temperatures through the depth of concrete deck in location 5

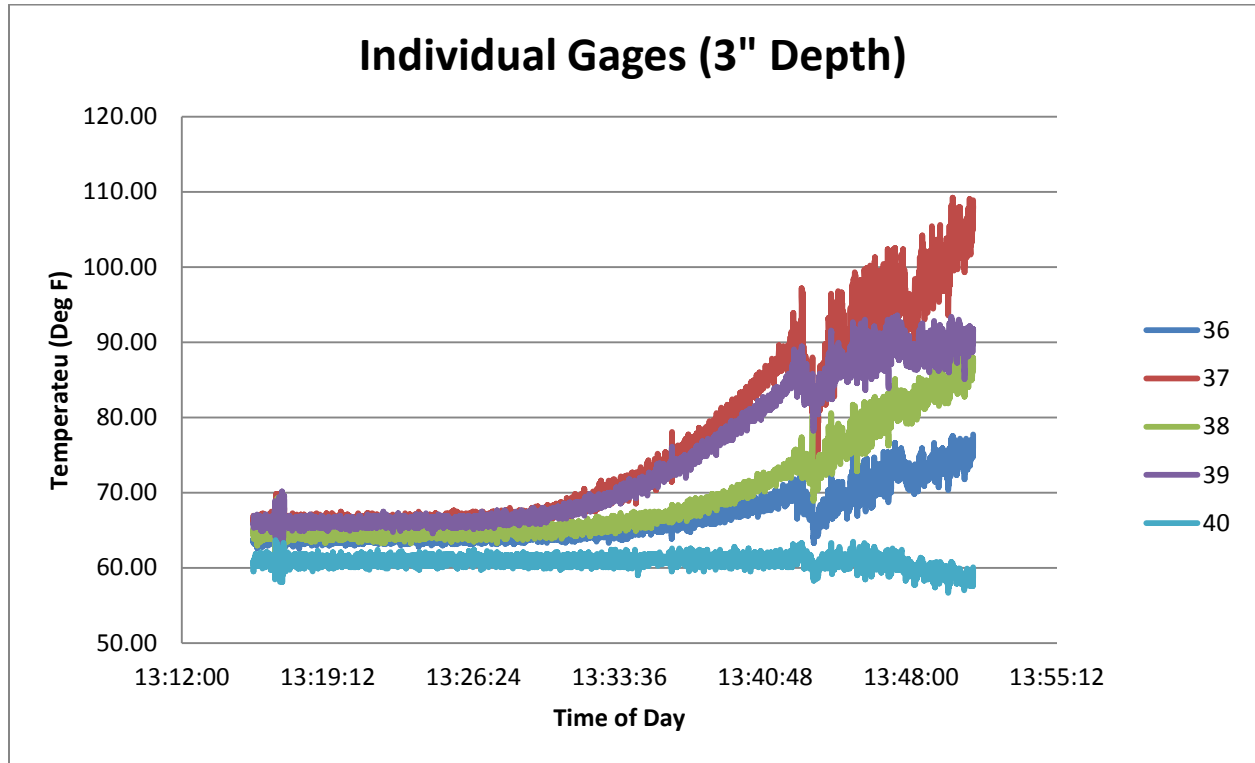


Figure 27 – Individual embedded thermocouples (3” from bottom face of deck)

Composite Arch Bridge

Deflection, air temperature and deck temperature were also recorded throughout the hour long test of the composite arch bridge specimen. The interior of the burn chamber during the test can be seen in Figure 28. This extent of flames was not seen in the steel bridge test. The embedded gages were in similar locations with the exception of gage 40, which was not included in this test. The same fourteen (14) air temperature gages were used in the chamber and the results can be seen in Figure 29. Plots of deck temperature can be seen in Figure 30 through Figure 35. A plot comparing midspan deflection of the steel and concrete arch bridge with the hybrid FRP composite bridge is shown in Figure 36.



Figure 28 – View through peep sight into chamber during composite arch burn test

The burner did not need to be cycled as in the steel bridge test as temperatures were near the temperatures of the previous test with the burner on low. Smoke production during the test peaked and then dissipated towards the midpoint of the test. The burner was cycled to high during the last 10 minutes of the test. Smoke production and crown deflections increased slightly during this time with increased temperature.

The day of the composite bridge test was a partly cloudy, warm day. There was no rain as experienced during the steel bridge test.

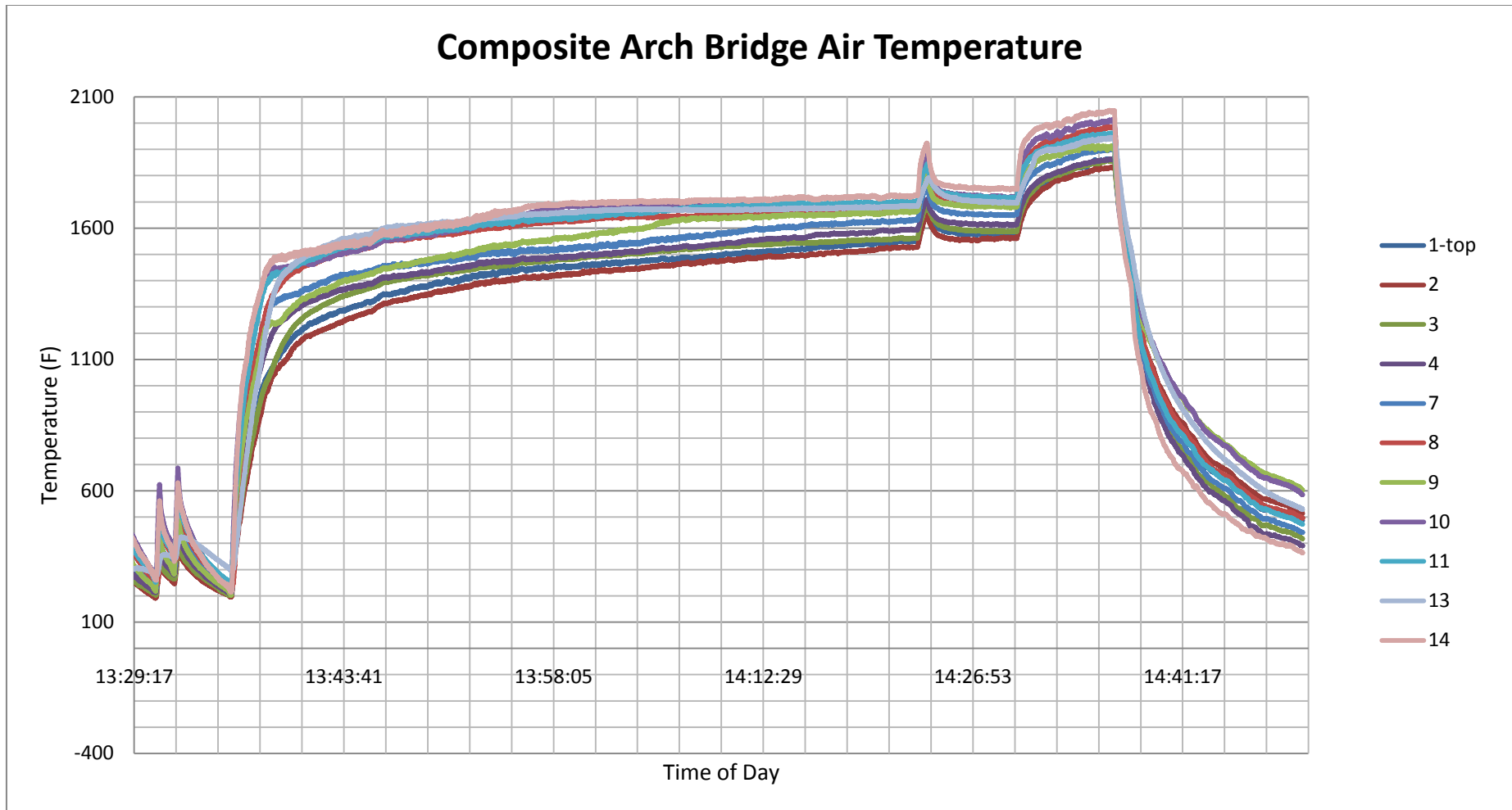


Figure 29 – Air temperature during heating of hybrid FRP composite bridge

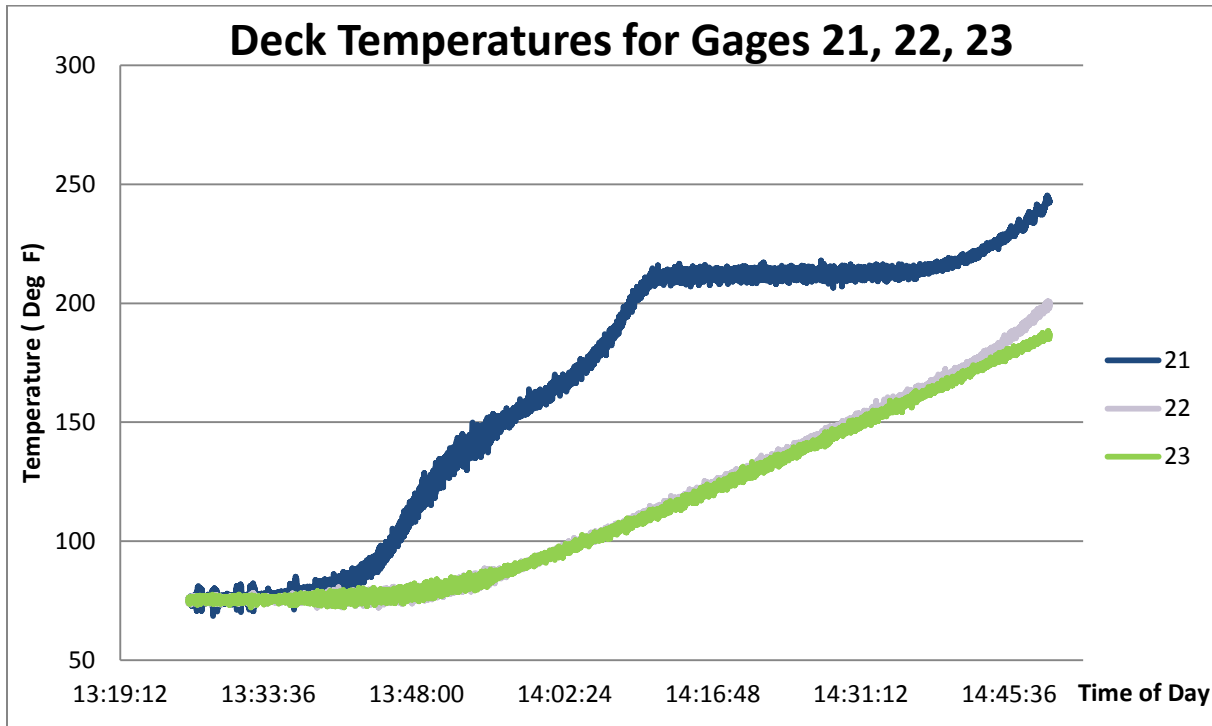


Figure 30 – Temperature versus time for gages 21-23 in concrete deck of FRP arch bridge

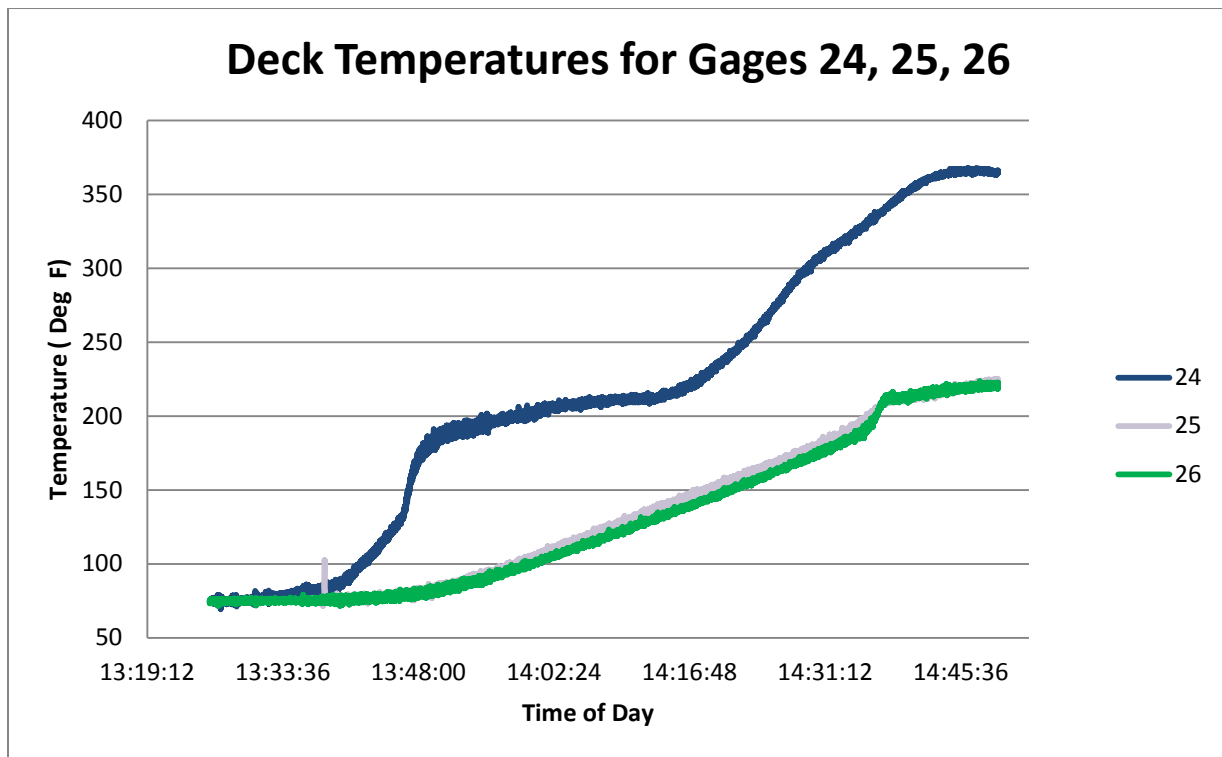


Figure 31 - Temperature versus time for gages 24-26 in concrete deck of FRP arch bridge

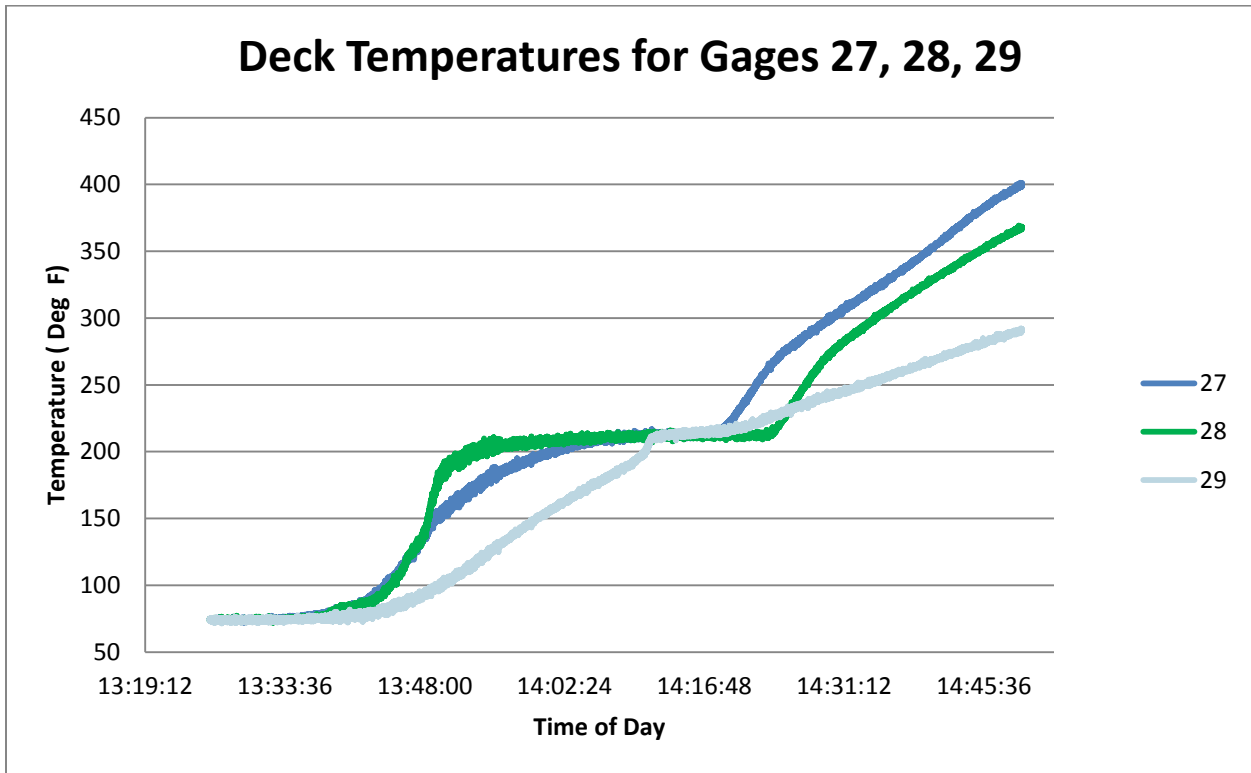


Figure 32 - Temperature versus time for gages 27-29 in concrete deck of FRP arch bridge

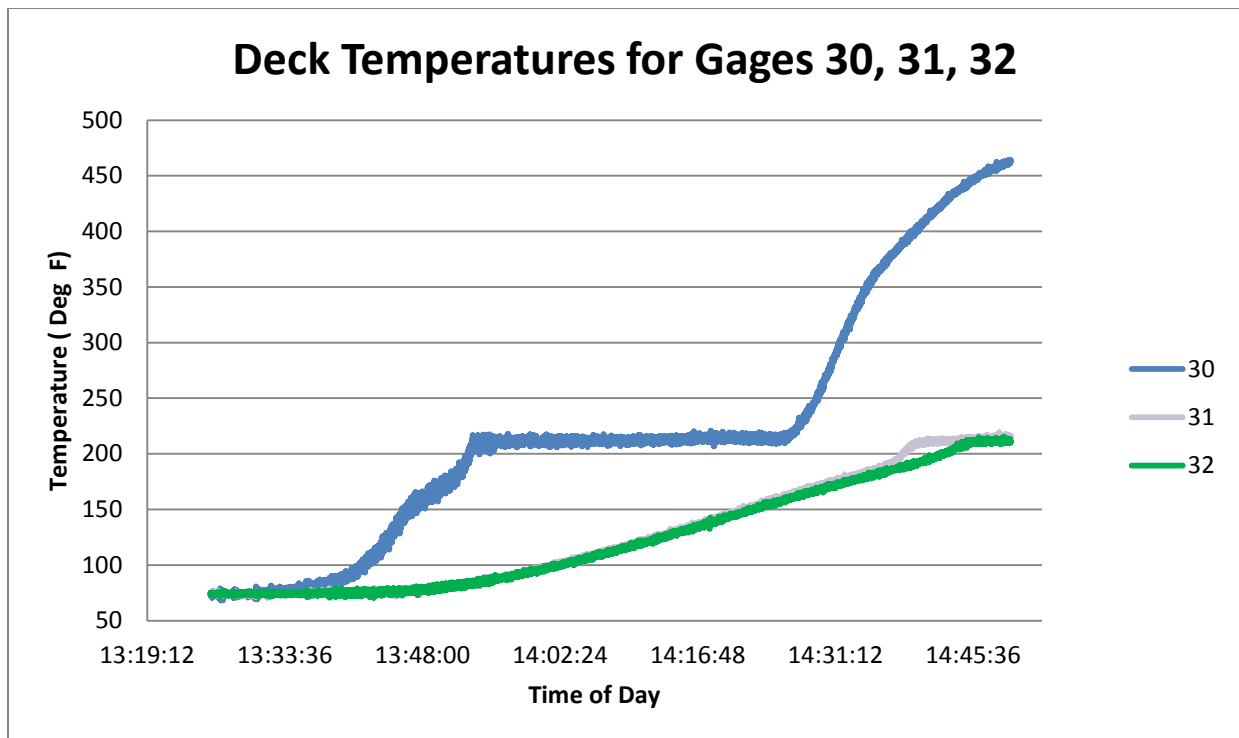


Figure 33 - Temperature versus time for gages 30-32 in concrete deck of FRP arch bridge

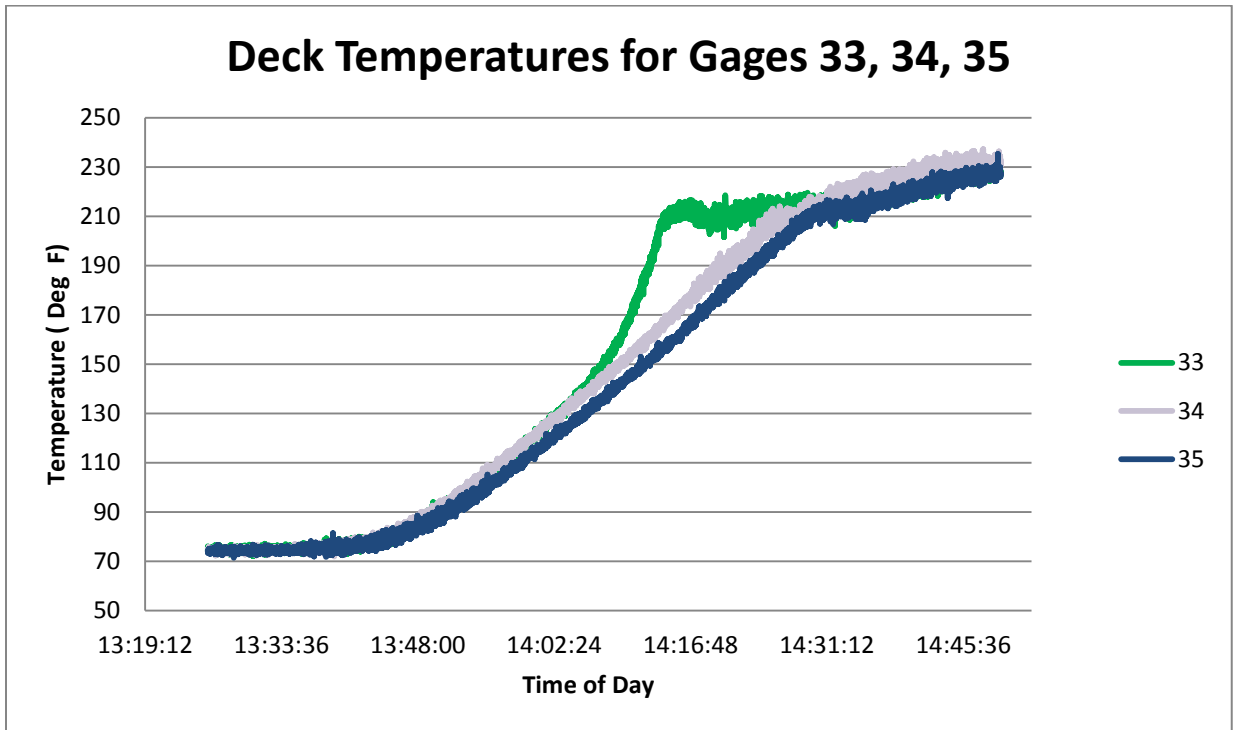


Figure 34 - Temperature versus time for gages 33-35 in concrete deck of FRP arch bridge

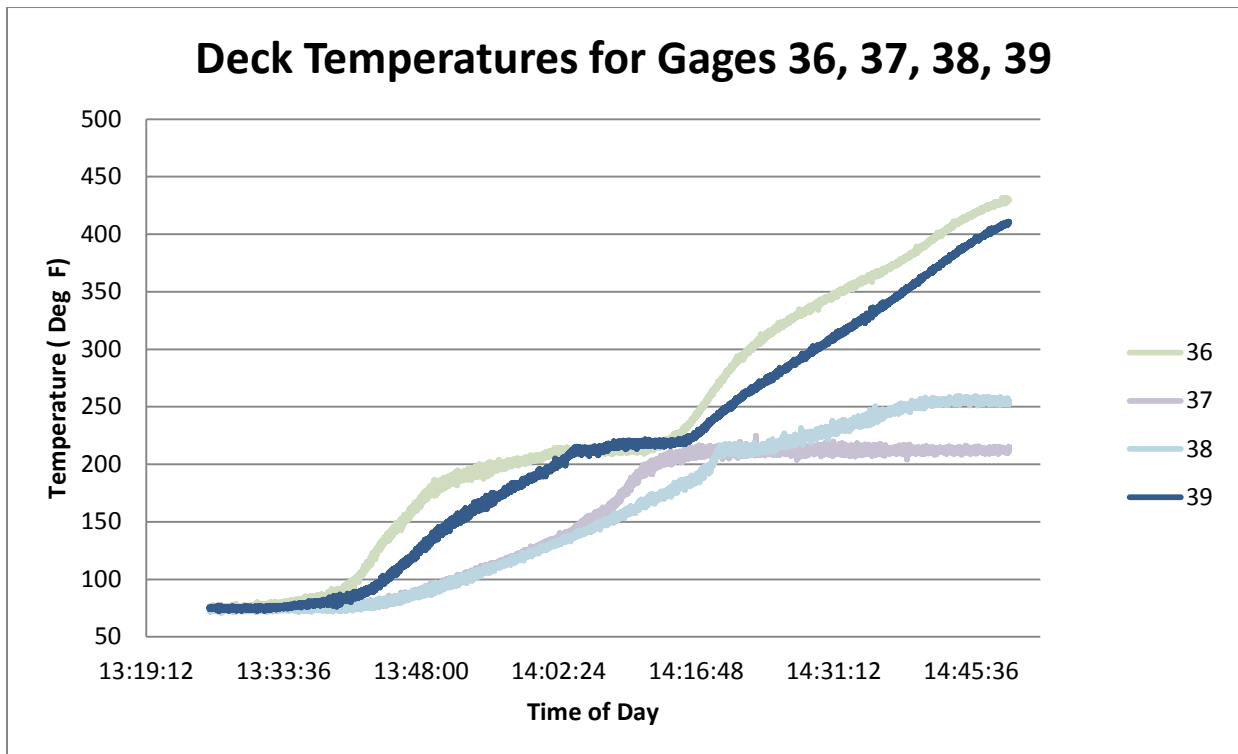


Figure 35 - Temperature versus time for gages 36-39 in concrete deck of FRP arch bridge

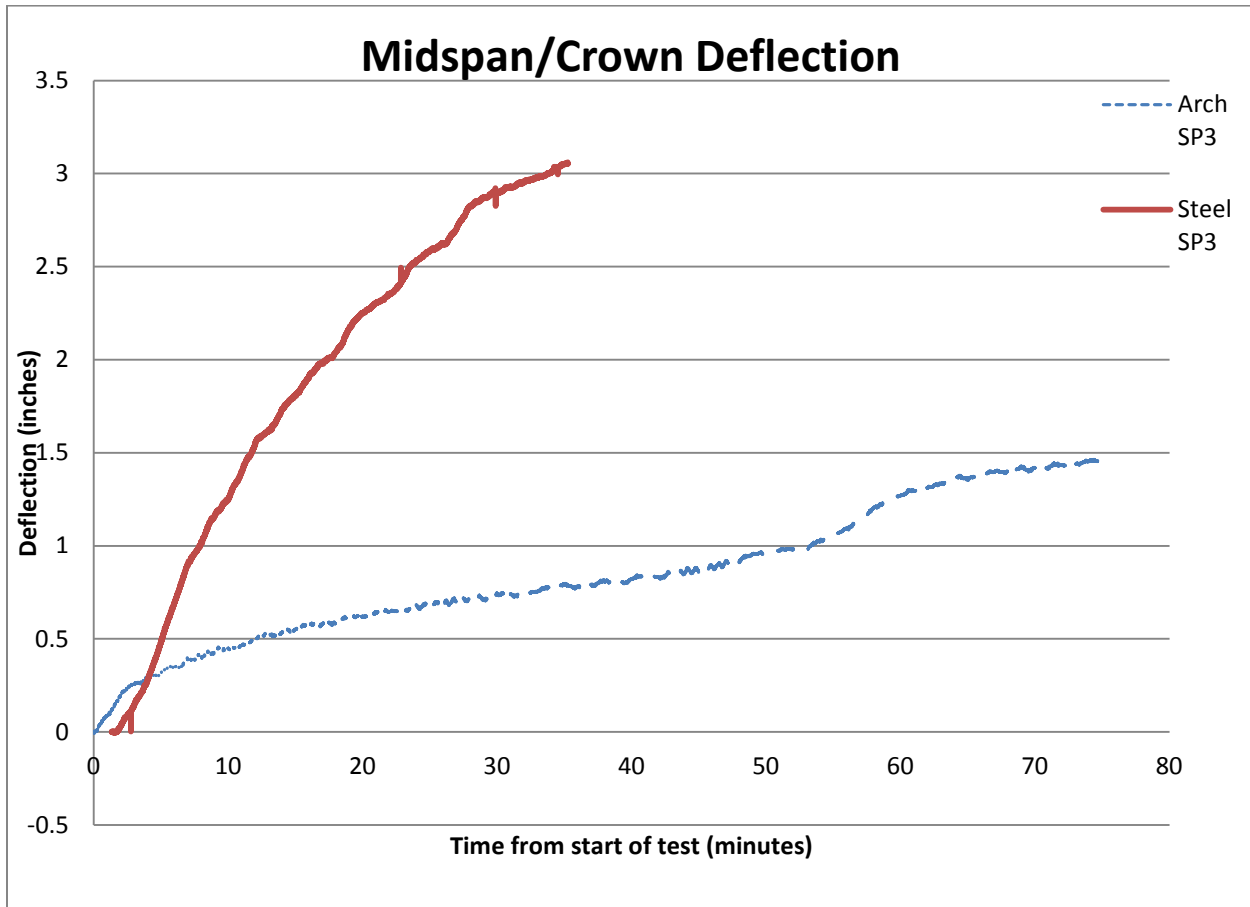


Figure 36 – Deflection of midspan string pot during test

DISCUSSION AND SPECIMEN CONDITIONS POST TEST

Both the steel bridge and composite bridge sustained the applied load during the burn test. The steel bridge and composite bridge results, including the condition after the test, are discussed and highlighted.

The steel bridge did not ultimately fail during the test, but the test was stopped due to excessive deflections of approximately 3 inches at midspan. Additional deflections would have caused damage to the test chamber and compromised the ability to test the composite arch bridge. The ability of the steel bridge to carry the load after the steel had reached temperatures that would reduce its yield strength below the calculated steel stresses, was initially somewhat surprising. However, the longitudinal bending strength of the concrete deck alone was not initially accounted for in the calculation of steel stresses and predictions of bridge behavior. In the design of the test specimen, minimum deck thicknesses were followed according to AASHTO LRFD bridge design specifications (AASHTO 2012), which led to an atypically high ratio of deck thickness to section depth. As a result, even with most of the steel wide flange section yielded the bridge deck and top flange of the girder were able to carry the load when the deck was at typical operating temperatures as shown in Figure 22 through Figure 27. Specimens with more typical ratios of deck thickness to section depth might lose the ability of carry the design

test load unlike the test specimen used here. However, the use of a relatively thick deck that matches normal bridge construction is justified since it ensures that the thermal mass of the deck represents field conditions, and that the deck draws heat from the girders and heat source at a rate consistent with actual construction. This greater thermal mass will also tend to slow or reduce heat buildup in the girders, prolonging their stiffness and strength retention, and therefore providing a more conservative basis for performance comparison between the arch and steel girder bridges.

Following the test, the steel girders and deck showed permanent deflections that appeared to be less than the maximum deflections seen during the test as would be expected from contracting steel beams as they cooled and reduced curvature. The bridge specimen can be seen after the test in Figure 37. No spalling of the deck or other damage was witnessed as seen in Figure 38.



Figure 37 – Longitudinal deflections in steel girders following the test



Figure 38 – View under bridge from within the chamber shortly after the steel bridge test

The composite arch bridge showed more obvious deterioration to the arch members due to the heat. Significant smoke production was seen during the test though it reduced in volume until the burner was turned on high (Figure 39).



Figure 39 – Arch bridge test smoke production

Figure 40 shows the interior of the bridge after the test. It appears most of the resin had burned off and the braided carbon fiber was dry and clean to the touch and loose around the concrete core of the arches. This extended to where the arch extended through the insulation in the chamber as seen in Figure 41.

The decking showed significant deterioration as seen in Figure 40. It was dry and brittle when removed from the arches in the lab. Charring can be seen on the underside and discoloration on the top of the decking. Additional photos of the decking can be seen in Figure 42 and Figure 43.



Figure 40 – Interior of bridge post test



Figure 41 – Arches at interface with chamber



Figure 42 – Underside of decking after removal from the arches



Figure 43 – Underside of second decking panel after removal from arches

The inner glass layer was inspected following the laboratory structural testing when the arches were cut open and layers within the arch were investigated. The carbon fibers appeared as if they were a new fabric prior to manufacturing. The inner glass layer was heavily charred, weak and brittle. The black inner glass layer can be seen in Figure 44. Samples were taken and could

be pulled apart by hand parallel to the dominant fiber direction (approximately the hoop direction).



Figure 44 – Inner glass layered charred under the dry carbon fiber

Arch crown deflections in addition to that shown in Figure 36 due to dead load, contributed to horizontal movements of the footings as seen in Figure 45. The self-reacting system consisted of steel cables and steel channels bending about their weak axis. The steel channels were not stiff enough due to the offset and overhang required to move the burner in and out of the chamber opening, Figure 46.



Figure 45 – Horizontal movement of footings during test



Figure 46 – Self-reacting system with overhang opposite burner

The arch bridge was also not buried as they normally are for all highway bridges to date. This would provide additional restraint to the arches shape. There would also be additional dead

load. The test is generally believed to be a conservative representation of the capacity of the arches during fire exposure.

CONCLUSIONS

Two bridges were constructed to carry HL-93 loadings and were tested under extreme heating conditions for the middle 6 feet of their spans while carrying a live load of approximately 25% of their reserve capacity, which is the nominal moment capacity minus the moment due to the self-weight for this test.

Deflections limited the test duration for the steel bridge, so that collapse was not observed. More typically sized steel girder and concrete deck bridges have smaller ratios of deck to total section height and would not be expected to perform as this test specimen did. Steel temperatures were very high, as evidenced by their glowing red color, which reduced yield strengths to levels below the stresses seen across a significant portion of the cross section of the girder.

The composite arch bridge performed well during this test with conservative conditions for footing and arch support and live loading. Real world loading will be better distributed and confining pressures of the soil will better support the in-place arches and serve as a heat sink reducing temperatures on the structure. Even with all of the resin burned off of the center portion of the span, the arches had minimal deflections and continued to carry the load applied. This allowed the arch bridge to have individual arches tested for reserve capacity in the laboratory. However, it must be noted that post-test inspections indicated that the inner glass layer of the hybrid glass-carbon shell suffered more significant fire degradation than the outer carbon layer. This indicates that the all-glass arches may not perform as well under fire as the glass-carbon system tested here.

LABORATORY STRUCTURAL TESTING OF LARGE SCALE TESTING

OBJECTIVE

Additional structural testing was planned that investigated residual capacity of the arches after they were exposed to extreme temperatures under load. This additional laboratory testing was beyond the proposed scope of work but prudent given the performance of the arches in the field testing.

TEST SETUP AND INSTRUMENTATION

Following the field testing, the arch bridge was shipped back to the Advanced Structures and Composites Center. Once back at the Composites Center, the bridge was prepared for testing and instrumented under a 110 kip servo-hydraulic actuator where three of the four arches were tested individually to failure.

The arch bridge was returned to the structural testing lab as a whole part with four arches embedded in one concrete footing at each end of the span along and with composite and concrete decking attached to the middle six feet of the span as seen in Figure 47.



Figure 47 – Bridge test specimen returning to structural testing lab

The concrete and composite decking was removed from the arches so that individual arches could be loaded at their crown by the actuator. Photos showing the condition of the composite decking can be seen in Appendix B.

Each of the arches was tested as they stood in the concrete footings. During the testing process, the bridge was slid sideways (transverse bridge direction) 18 inches to allow for the centerline of

the arch to be tested underneath the actuator. The width restraints of the test frame did not allow all four arches to be tested this way however. One of the arches was removed to allow for the opposing outer most arch to be tested as seen in Figure 48. The arch showing the least degradation to the heat was removed from the footing and not tested.



Figure 48 – Arches prior to testing under test frame

The arches foundations were tied as they were in the field testing with cable, threaded rod and steel channel as a self-reacting system. Foundations were not restrained against rotation other than the self-weight of the foundations.

Instrumentation included string pots at the midspan, the shoulders, and the footings in order to measure the crown vertical deflections, the shoulder horizontal and vertical deflections, and the footing spread, respectively (Figure 49).

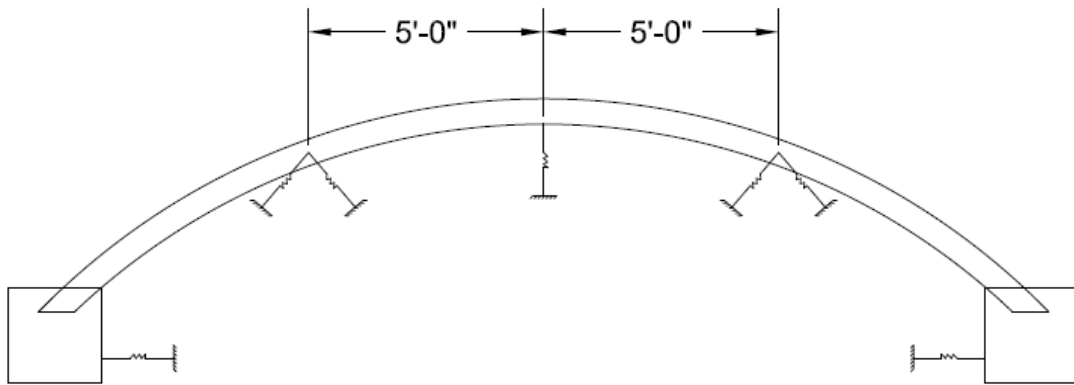


Figure 49 – String potentiometer locations

Two string pots were used at the shoulders at a measured angle to capture horizontal and vertical deflections of the mid-height of the arch. This can be seen in Figure 50.



Figure 50 – String potentiometers at shoulders

Load was captured with a calibrated 110 kip load cell at the crown of the arch where a single patch load (9 inch long and 12 inch diameter arc) was applied. Load was applied at the crown downward at a constant rate of 0.35 inches per minute until failure.

RESULTS

The three arches failed in similar modes which was bending failure at the shoulder where relatively undamaged laminate met the section of the arch inside the chamber during the field test. A typical failure of the three arches can be seen in Figure 51.



Figure 51 – Typical arch failure at shoulder during structural testing

Arch load and deflection data at the crown is plotted for each arch in Figure 52.

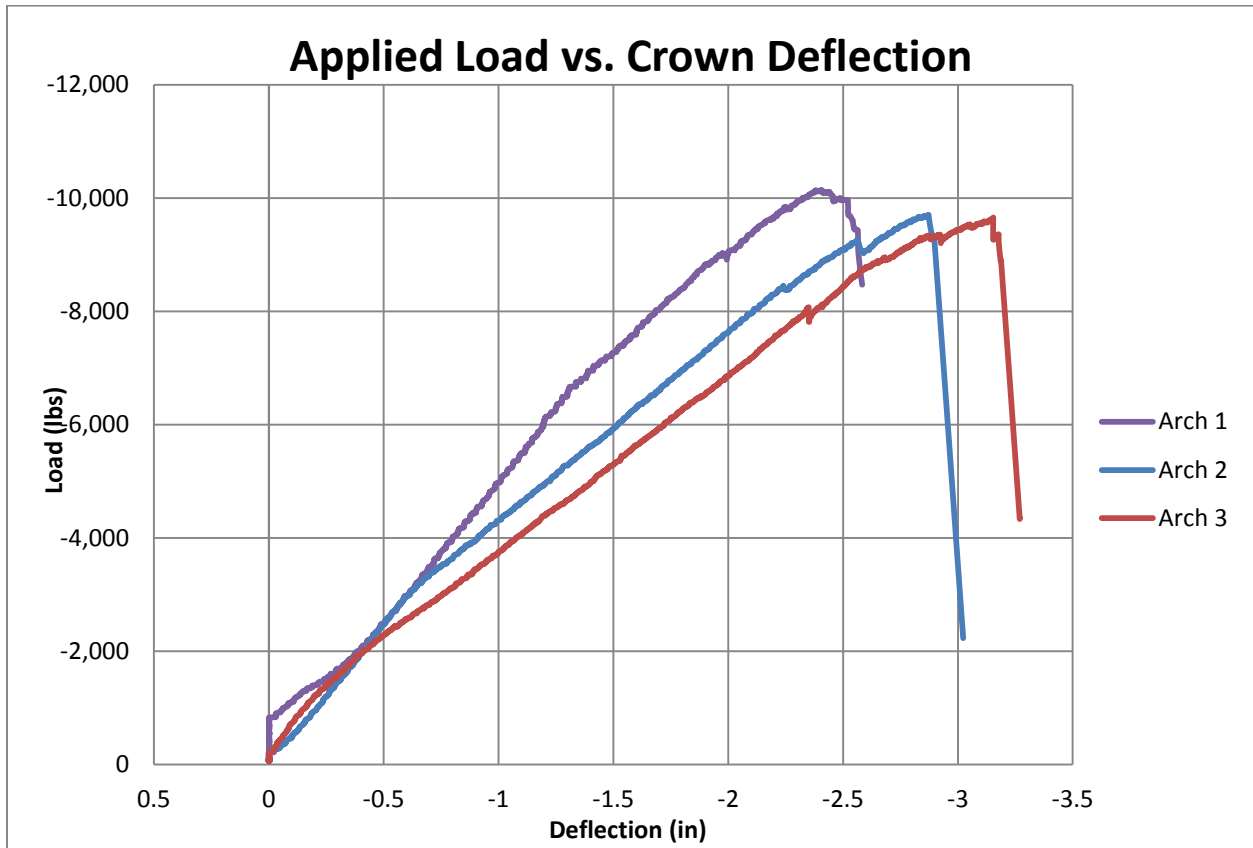


Figure 52 – Load versus deflection plots of each arch during structural testing

Footing deflections were also measured to document spreading of the arch base during testing as this was not a true pin or fixed condition. Outward spreading of the footings can be seen in Figure 53 where spreading of the North footing can be seen as positive values and spreading of the South footing with load can be seen as increasing negative values.

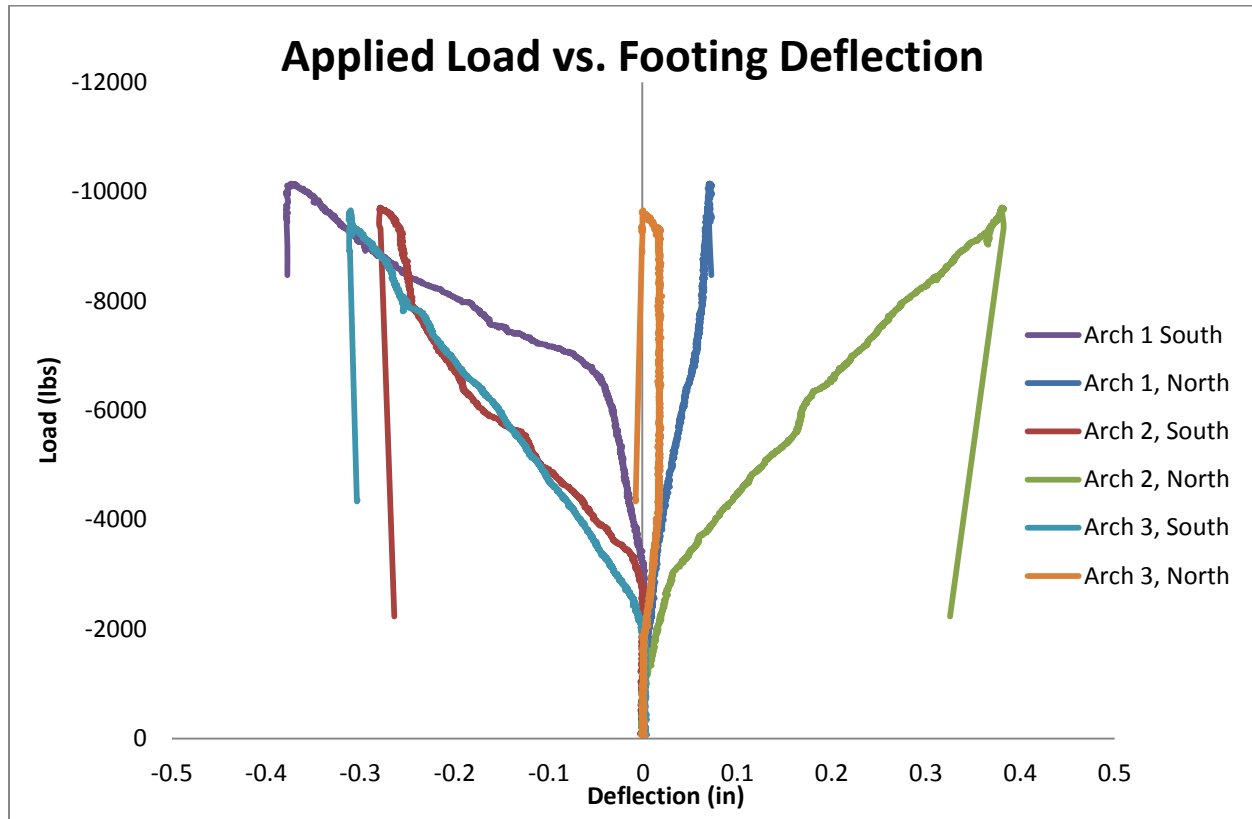


Figure 53 – Footing deflections

Vertical and horizontal deflections of the arch quarter points in span are shown in Figure 54 and Figure 55.

A RISA-3D model was created of the single arches during the structural testing to estimate the flexural forces in the arch during the test. A plot of the bending moment with the crown loads and footing restraint depictions are shown in Figure 56. A distributed load over the 9 inch length of the load head is shown with pin supports for vertical and out of plane displacements of the footings. Springs were added and calibrated to best match the measured footing spread at the peak load. The total load in the model corresponded to the peak load in the test. Constant material properties were used across the arc length.

A peak vertical moment was found to be approximately 122.5 kip-in, though there appeared to a significant side load as well due to the asymmetric damaged section. This occurred at the crown where it appeared the resin had been burned off. Peak moments during the test at the shoulders (5 feet from midspan) were interpolated from the results to be 45.5 kip-in.

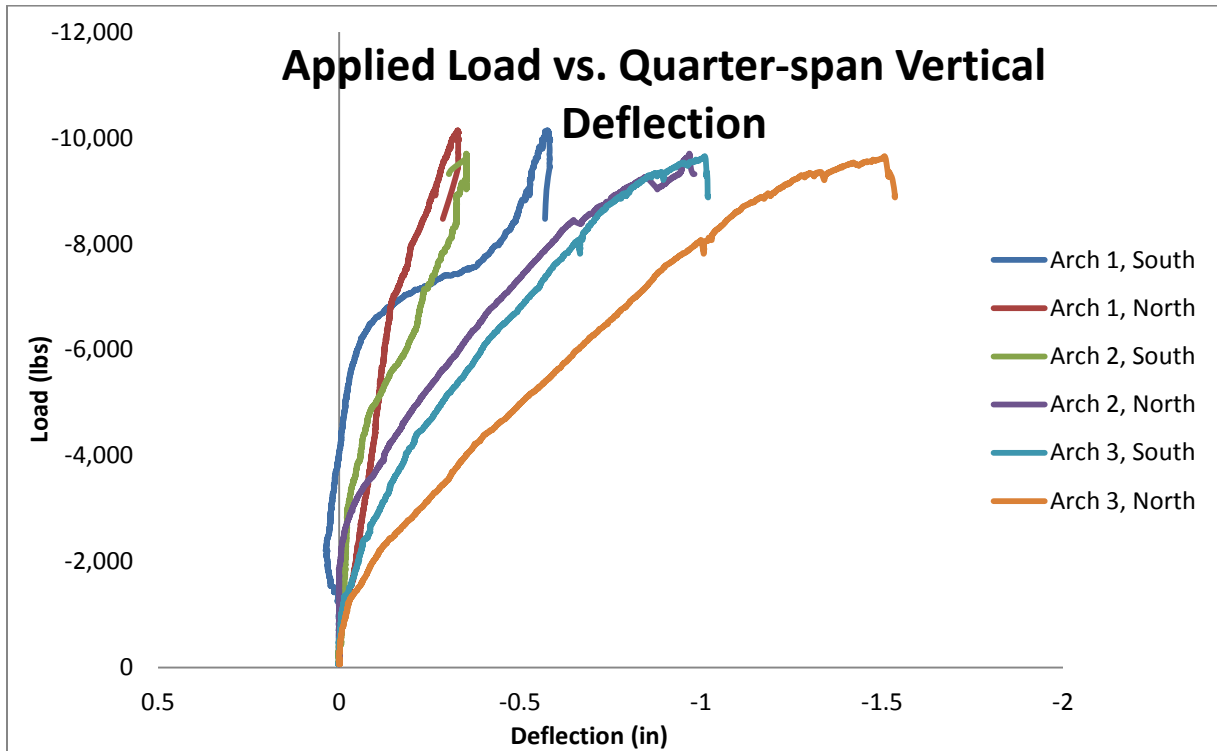


Figure 54 – Load versus shoulder vertical deflection

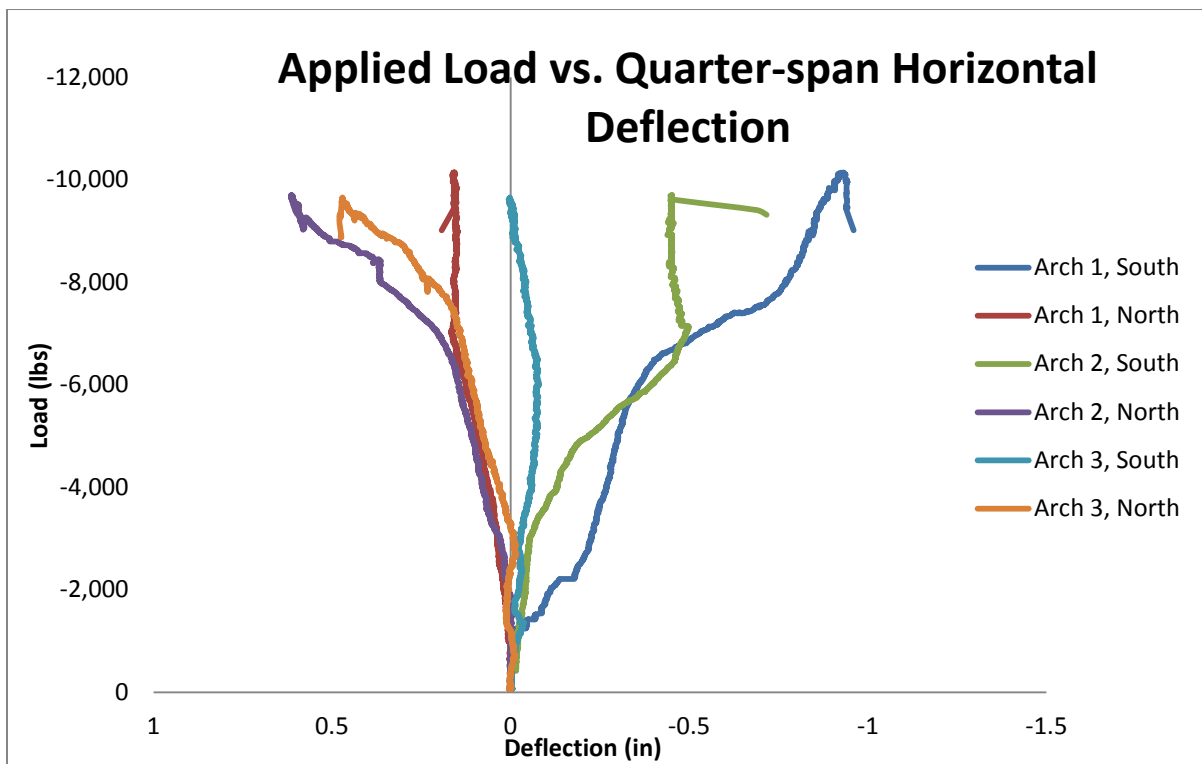


Figure 55 – Applied load versus arch shoulder horizontal deflection

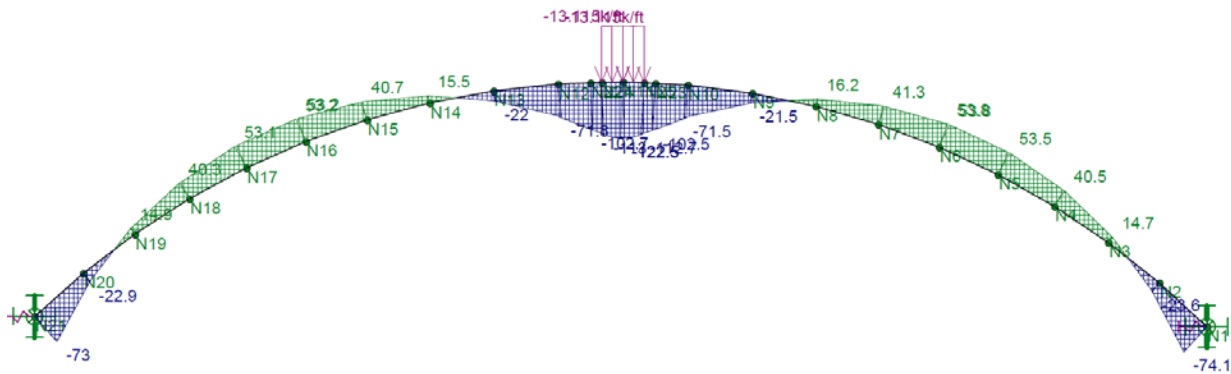


Figure 56 – RISA 3D model analysis estimating moment during test

DISCUSSION AND CONCLUSIONS

Structural testing of the fire damaged arches was performed to supplement the field testing. The nature of the damage to the arches did not permit the specimens to incorporate the traditional higher quality of instrumentation and data collection. Asymmetric and out of plane loading was seen during the test that would be assumed to show lower failure loads than actually calculated. Peak moments from the calculations correspond to the crown of the arch under the load head, but failures were seen where the “softer” fire damaged section transitioned to the more rigid, less damaged arch section. This cross section was near the wall of the fire chamber and was insulated from the heat of the chamber.

Failures at the shoulders also appeared on the outside tension face of the arch and showed less obvious failures than seen in other structural arch tests. This could be due to the degradation of the inner glass layer, the removal of resin from the damaged area of laminate during the burn test, or other reasons.

It is difficult to quantify capacities of this transition region of the arch. Modeling the member with constant material properties also gives lower bounds for the moment at the point of failure during the structural testing. With that lower bound, the ratio of failure moment to capacity for this cross section is estimated to be at 0.243 (45.5 kip-in/ 187.2 kip-in capacity).

The laboratory structural testing demonstrated there is structural capacity remaining in the arches after approximately one-third of the span was exposed to extreme heat, which appeared to burn off 100% of the resin in the laminate.

REFERENCES

- American Association of State Highway Transportation Officials (AASHTO). (2012). AASHTO LRFD Bridge Design Specifications, 6th edition with interims. Washington DC: American Association of State Highway and Transportation Officials.
- American Association of State Highway Transportation Officials (AASHTO). (2012). AASHTO LRFD Guide Specifications for Design of Concrete-Filled FRP Tubes, 1st Edition. Washington DC: American Association of State Highway and Transportation Officials.
- ASTM, A. S. f. T. M. (2008b). "ASTM D 3039: Standard Test Method for Tensile Properties of Polymer Matrix Composite Materials." ASTM International, West Conshohocken, PA.
- Burgueño, R. (1999). System Characterization and Design of Modular Fiber Reinforced Polymer (FRP) Short- and Medium-Span Bridges. (Doctoral dissertation, University of California, San Diego, 1999). (UMI No. 9928617).
- Davids, William, et al. Response of Concrete-Filled Tubular FRP Arches to Construction-Induced Loading. 29th International Bridge Conference. IBC 12-109. June 10-13, 2012. Pittsburgh, PA.
- U.S Department of Transportation, and Federal Aviation Administration. (2000). "Aircraft Materials Fire Test Handbook." National Technical Information Service, Washington, D.C.

APPENDIX A – CASE STUDY: DESIGN CALCULATIONS FOR EXTREME EVENT II LOADING WITH REDUCED MATERIALS PROPERTIES

A case study was performed to evaluate a bridge using material properties from the coupon testing to evaluate the ability of the bridge to carry loads in the Extreme II load case (AASHTO 2012) with reduced material properties from the coupon testing. The case study uses a representative hypothetical 40 foot span bridge with 12” diameter carbon fiber hybrid composite arches spaced at 5 feet with a 15 foot rise and fixed foundations.

Analyses were conducted with a 2D beam finite element model created at the Composites Center with earlier versions documented in Davids et al 2012. Service moments, shear and axial loads, and deflections were output for various parts of the loading DC, DW, LL, etc and then the applicable load factors were applied for Strength I and Extreme II.

Peak moments for the model occurred at the footings, but were neglected as they would be reinforced with an internal rebar cage in service. Internal moments were focused on, and compared with, bending capacities of cross sections with full capacity and with the tensile capacity of the laminate reduced by 50%. Section moment capacities were calculated according to Burgueno and Bhide 2006, and calculated at the minimum axial load. A summary of the results is presented in Table A1.

Table A1 – Summary of Case Study Analysis

	ϕ Mn (kip-in)	Mu (kip-in)	Pu_min (kip)	Pu_max (kip)	Vu (kip)
Strength I	532.1	495.3	108.3	199.4	22.1
Extreme II	<i>399.7</i>	<i>322.3</i>	108.3	152.2	17.8

For this hypothetical case the arch bridge system was slightly overdesigned for internal moment for the Strength I load case, but also was over designed by a higher degree for the Extreme II loading case where tensile capacities of the laminate were reduced by 50%.